Measuring and Modeling Fault Density for Plume-Fault Encounter Probability Estimation

Preston D. Jordan[1*], Curtis M. Oldenburg[1] and Jean-Philippe Nicot[2]

[1]Earth Sciences Division
Lawrence Berkeley National Laboratory
Berkeley, California 94720

[2]Bureau of Economic Geology
Jackson School of Geosciences
University of Texas
Austin, Texas 78713

Abstract

Emission of carbon dioxide from fossil-fueled power generation stations contributes to global climate change. Storage of this carbon dioxide within the pores of geologic strata (geologic carbon storage) is one approach to mitigating the climate change that would otherwise occur. The large storage volume needed for this mitigation requires injection into brine-filled pore space in reservoir strata overlain by cap rocks. One of the main concerns of storage in such rocks is leakage via faults. In the early stages of site selection, site-specific fault coverages are often not available. This necessitates a method for using available fault data to develop an estimate of the likelihood of injected carbon dioxide encountering and migrating up a fault, primarily due to buoyancy. Fault population statistics provide one of the main inputs to calculate the encounter probability. Previous fault population statistics work is shown to be applicable to areal fault density statistics. This result is applied to a case study in the southern portion of the San Joaquin Basin with the result that the probability of a carbon dioxide plume from a previously planned injection had a 3% chance of encountering a fully seal offsetting fault.

[*] Corresponding author: E-mail: pdjordan@lbl.gov; phone: (510) 486-6774; Fax: (510) 486-5686

Introduction

Fossil-fuel fired electrical power plants emitted 41% of the carbon dioxide due to energy usage in the United States in 2008 (EIA, 2009). Storage of a portion of this carbon dioxide in the pore space of geologic strata (geologic carbon storage) is one possible mitigation for the portion of climate change otherwise attendant upon emitting this pollutant to the atmosphere.

Geologic carbon storage is envisioned in both strata from which oil and/or gas have been produced as well as strata containing primarily saline waters, termed saline aquifers. If geologic carbon storage is to be a significant mitigation, storage in saline aquifers is necessary because the volume of the depleted oil and gas fields is not sufficient relative to the quantity of carbon dioxide emitted from large, fixed sources. This is due to the burning of coal sourced from the near surface by most large, fixed sources as well as the relatively lower volumetric density of carbon in carbon dioxide as compared to fossil fuels.

Leakage of stored carbon dioxide out of designated subsurface storage volumes is one of the main concerns regarding geologic carbon storage. For example, carbon dioxide could migrate from a storage site into a hydrocarbon resource, such as a natural gas deposit. Fault zones are considered one of the main potential leakage pathways (Benson and Cook 2005). For such leakage to occur carbon dioxide must both encounter a fault and the fault must be relatively more transmissive than the surrounding rock. Certainty about the location and character of fault zones varies from higher in depleted oil and gas reservoirs to lower in saline aquifers. Consequently a more deterministic assessment of leakage risk due to faults is possible for storage in mature oil and gas reservoirs and a more probabilistic assessment is necessary for saline aquifers, particularly in the early site selection phase of a project.

Two inputs are needed for assessing the probability of a carbon dioxide plume encountering a fault – the footprint of the plume and fault statistics (Jordan et al. 2011). The smaller the footprint and/or the smaller the fault density, the smaller the likelihood the plume will encounter a fault. Numerical modeling can provide realizations of the plume footprint. Available fault coverages can provide an understanding of the fault population.

This paper develops a more readily usable fault statistical approach applicable to geologic carbon storage, and applies that approach to develop fault statistics from publicly available coverages for input to a plume-fault encounter probability estimate for a proposed storage test site: the Western Regional Carbon Sequestration Partnership's (WestCarb) Phase III injection site at Kimberlina northwest of Bakersfield, California. The injection horizon for this planned experiment is a saline aquifer for which there is little publicly available data regarding faulting. There are numerous oil and gas fields in the vicinity with publicly available structure maps, however. Statistics regarding fault orientation and fault population are developed from these coverages allowing calculation of the probability the planned Kimberlina carbon dioxide plume will encounter a fault.

Background

Numerous investigators have found that fault length and displacement populations can often be represented by a power-law distribution. This finding is based upon field research (e.g., Watterson et al. 1996), physical modeling (e.g., Ackerman et al. 2001), and numerical simulations (e.g., Cowie et al. 1995). Power-law distributions are of the form

$$N \propto aS^{-C} \qquad (1)$$

where N is the number of faults of a size greater than S, and C is the power law exponent (notations from Watterson et al. 1996). For instance, N can represent the number of faults greater than a certain length determined from a two-dimensional sample space, such as a geologic map. Alternately, N can represent the number of faults with greater than a certain displacement, d, encountered in a one-dimensional sample space, such as a scan line. When d (known as the displacement cutoff) is substituted for S, Equation 1 becomes

$$N_d \propto d^{-C_d} \qquad (2)$$

where the subscript "d" is for displacement cutoff.

Field studies, numerical simulations, and physical modeling have also indicated that at very low strains and high strains, fault density versus throw truncation is exponential rather than power law (Cowie at al. 1995 and Ackermann et al. 2001). They also show that C_d declines with increasing strain during the initiation of faulting, and becomes constant with further strain. At initiation of strain, many small faults develop, and so C_d is large. As strain continues, some of the faults grow and eventually link, while few new small faults develop, so C_d decreases. Values reported in the literature are likely to emphasize lower values for C_d as field studies are easier to carry out on more heavily faulted terrains. At very high strains, further development of one fault tends to dominate, and the fault population evolves toward a "characteristic" fault population, akin to a characteristic earthquake population.

Fault Density Approach

If N represents the number of faults greater than a certain length, it is often difficult to measure in practice due to the confounding effects of fault intersections. Further, the orientation

of the boundary of a fault coverage can introduce scatter in the fault density distribution measured from the coverage.

The areal density of faults, *F*, with a certain value of *d* is easier to measure. It can be accurately calculated by measuring the length of faults with greater than a certain displacement occurring in a coverage area and dividing by that area. It avoids handling of fault intersections inherent in defining the number of faults based on length, and it does not suffer from bias introduced by the orientation of coverage margins. Use of *F* is workable because it is proportional to N_d, as shown following, so can be substituted for N_d in Equation 2.

N_d can be multiplied by the average length of fault (l_d) represented by each fault intersection with one of multiple scan lines across a coverage. This value is proportional to the average sample-line spacing. Multiplying N_d by l_d yields

$$l_d N_d = L \tag{3}$$

where *L* is the total length of faults with *d* greater than a particular value. Obviously, *L* can be directly measured from a fault map rather than through scan lines. Multiplying Equation 2 by l_d yields

$$l_d N_d \propto d^{-C_d} \tag{4}.$$

Substituting Equation 3 into Equation 4, and dividing by the total area of the sample domain, *A*, gives

$$\frac{L}{A} \propto d^{-C_d} \tag{5}.$$

The value L/A is the fault density, *F*, so Equation 5 can be rewritten

$$F \propto d^{-C_d} \quad (6).$$

An additional implication of Equation 6 is that F follows the same pattern as N_d as strain accumulates.

Taking the log of Equation 6 gives

$$\log F \propto -C_d \log d \quad (7).$$

Equation 7 indicates a log-log plot of F against d will be linear if the fault population follows a power-law distribution. A semi-log plot of F against d will be linear if the distribution is exponential (very early stage or late stage strain).

Equation 7 implies that F approaches infinity as d approaches 0. In practice, most fault population researchers have found, or believe based upon theoretical considerations, that the relationship is accurate down to displacements equivalent to several grain diameters for clastic rocks (e.g., Ackerman et al. 2001). Even this implies F becomes very large at the actual lower limit of d. This suggests a high probability that a given CO_2 plume will encounter a fault of some size. Of course, most such faults will have such small displacements as to not be of serious concern in terms of leakage. Consequently, the concern for leakage should focus on faults of a certain size (large enough to have a high probability of leakage), rather than on all faults encountered as is often the case currently.

As defined above, F is a measure of fault density in a two-dimensional space. As such, F provides a biased estimate of the fault density in the three-dimensional rock volume (Pickering et al. 1995). Due to the buoyancy of CO_2, and typically much greater length and width than thickness of most proposed storage reservoirs, carbon dioxide plumes will typically be more two-

than three-dimensional. As a result, F is the proper parameter for estimating the probability of a CO_2 plume encountering a fault with a given displacement.

However, three-dimensional fault density can enter back into consideration several steps after a plume encounters a fault. After such an encounter, the first issue is the flow and transport properties of the fault. If these properties are such that leakage via the fault can occur, then the next relevant issue is the vertical extent of the portion of the fault with these properties. If the extent of this portion of the fault is sufficient to allow leakage all the way from the CO_2 plume to a volume of concern (i.e., a receptor such as an underground source of drinking water (USDW)), then analysis should proceed to consideration of impacts. If the extent of the leakage-capable portion of the fault is insufficient to allow direct leakage to a receptor, but sufficient to allow leakage out of the storage formation, then consideration of leakage via more complex pathways must occur. This network is defined in part by the three-dimensional fault density, along with the distribution of permeable geologic units in relation to the fault density. Such considerations are outside of the current study, but the probability of flow through conductive fault networks with power-law populations is developed in Zhang et al. (2010).

Fault Encounter Probability

The other input to calculating the probability of a plume encountering a fault of a particular size is half the plume dimension perpendicular to the fault, k. This requires ascertaining the fault orientation mode from the fault coverages, as well as estimating the expected plume shape. The plume shape can be estimated from numerical simulations of the proposed carbon dioxide injection. With the fault density and fault perpendicular plume dimension, the encounter probability is calculated according to the equation

$$\Pr(g) = 2kF \qquad (8).$$

The derivation of this equation is given in Jordan et al. (2011).

If there is more than one fault strike mode, then multiple distributions of *F* will have to be defined based upon measurements from the fault coverage. Each mode will also require a different *k* unless the plume is radially symmetric. Equation 8 can then be used to calculate a Pr(*g*) for each mode for each fault size of interest.

Case Study: The Kimberlina Phase III Pilot Test

WESTCARB's Kimberlina Phase III pilot test project is located in the southern San Joaquin Basin in California about 27 km (17 mi.) northwest of Bakersfield, as shown on Figure 1. The San Joaquin Basin extends about 350 km (220 mi.) from the Stockton Arch to its southern terminus at the northern Transverse Ranges and averages 80–110 kilometers (50–70 miles) wide. It is bounded on the east by the Sierra Nevada and on the west by the Coast Ranges (NETL 2009). During the Mesozoic, the area was a fore-arc basin during subduction of the Farallon plate. By middle Tertiary time, the basin had become relatively isolated as a result of the transpressional margin that followed the passage of the Mendocino triple junction. The depositional environment generally progressed from deep marine in the Mesozoic to alluvial at present with a number of intervening transgression-regression sequences (Graham and Williams 1985).

During the Kimberlina Phase III pilot test, 1 Mt (10^6 t = 10^9 kg; $1.1*10^6$ T = $2.2*10^9$ lbs) of CO_2 was planned for injection into the Vedder sandstones over four years (NETL 2009). The Vedder consists of interbedded sandstones and shales deposited on the marine slope, shelf and delta comprising a ramp (Bloch 1986). At the site, the Vedder has a thickness up to 160 m (520

ft), and occurs at a depth of 2,300 m (7,500 ft) (Wagoner 2009). Thick continuous shale units provide good overlying seals at the site and surrounding areas (Wagoner 2009). Faults in the vicinity appear to be primarily growth faults (McPherson 1978).

Fault Data

Detailed information on faults at and in the vicinity of the Kimberlina site is not available. However, there are 27 oil and gas fields within 24 km (15 mi.) of the Kimberlina site where faults have been mapped extensively as shown on Figure 2. Structure maps from these fields provide a basis for predicting the likely pattern and occurrence of faults at the Kimberlina site. These maps are available in Volume 1 of "California Oil and Gas Fields" by the California Division of Oil, Gas and Geothermal Resources (DOGGR 1998, with the exception of the Rose Field for which no data were available). An example structure map is shown on Figure 3.

The contour interval of most of these maps is 15 or 30 m (50 or 100 ft). The minimum interval is 6 m (20 ft) and the maximum is 61 m (200 ft). The contour interval average is 23 m (76 ft), the standard deviation is 14 m (48 ft), the kurtosis is 1.85 and the skewness is 1.21. This indicates the distribution of contour intervals is relatively symmetric and peaked.

The orientation and length of 956 fault segments were measured from the maps. Throws, as annotated on Figure 3, were generally linearly interpolated from the structure contours. Throws at fault intersections were measured from the interpolated elevation of the fault-block corners. Throws were measured at 1,046 points. The total fault length measured was 465 km (289 mi). The resulting data are presented in Appendix 1.

The structure maps indicate almost all the fault segments were normal. Fault-dip information was not given on the maps, so only the throw (vertical component of displacement) could be measured. McPherson (1978) indicates most of the faults are vertical, at least upsection

from the Vedder, and likely subvertical at the Vedder. Therefore the throw is likely not much less than the dip component of displacement. As a result, measuring throw instead of dip displacement probably does not introduce significant errors.

Additionally, the offset perpendicular to bedding is likely more relevant to a fault's properties with respect to fluid flow than is the actual displacement as bedding perpendicular displacement is more related to the shale-gouge ratio. The shale-gouge ratio is the proportion of shale displaced past a particular point on a fault. Along fault permeability decreases with increasing shale gouge ratio, at least at lower values (Yielding et al. 1996). As the bedding dips in the vicinity of Kimberlina are generally small (7° for the Vedder Formation), the offset perpendicular to the bedding is almost the same as the throw, further justifying the focus on throw.

Fault Orientation

The distribution of fault orientations is shown on Figure 4. The primary mode is north to northwest. A secondary mode is to the northeast to east-northeast. The distribution of fault orientations in oil and gas fields centered within 16 km (10 mi.) of the Kimberlina site is shown in Figure 5. The primary mode of fault orientation is to the north. One third of the fault length occurs in this 10° interval. Three quarters of the fault length occurs in the north to northwest octant.

The distribution of fault orientations in oil and gas fields beyond 16 km (10 mi) but at least in part within 24 km (15 mi.) of the Kimberlina site is shown in Figure 6. The primary fault strike mode is to the northwest. About half of the fault length occurs in this mode. A fifth of the fault length occurs in a secondary northeast mode. A tenth of the fault length occurs in a tertiary north mode.

Comparison of Figures 5 and 6 indicates that fault sets with distinctly different orientation occur near the Kimberlina site versus farther away. This suggests that faults in the vicinity of the Kimberlina site will strike north to north by northwest.

Fault Data Aggregation

The field structure maps are constructed on a wide variety of stratigraphic horizons. Figure 7 shows that the faults in the vicinity of Kimberlina tend to persist through the pre-Pliocene Tertiary section, which includes the Vedder Formation (DOGGR 1998). The fault density for each field is defined as the field's total fault length divided by the area of each field's structure map.

The vertical distances from each mapped horizon to the Vedder Formation was measured from the geologic sections and/or stratigraphic columns available for each field (DOGGR 1998). Figure 8 shows the fault density from each structure map relative to the vertical distance from that horizon to the top of the Vedder. Relative map area is shown by symbol size.

The distribution of fault densities does not change appreciably within 1,500 meters (6,900 ft) of the Vedder. Data beyond this are sparse, but suggest the density may be lower. Still, the figure supports aggregating the fault data from all the maps for the purpose of fault encounter probability estimation.

Figure 9 shows the approximate direction and distance from the Kimberlina site to each field, the size of each field and the fault density in each field. The figure shows there are almost no fields from the northwest to northeast of the Kimberlina site. Further, the fault density is higher from the northeast to southwest, and lower from the southwest to northwest, despite a slightly higher concentration of fields with maps based on smaller contour intervals in the latter. Unlike fault orientation, though, there is no obvious trend in fault density with distance. These

data suggest that the Kimberlina site is in a transitional area between higher and lower fault densities.

Based upon Figure 9, the fault data from all the fields are aggregated for the purpose of calculating fault encounter probability in the Kimberlina area. Aggregation provides an average density that will account somewhat for the Kimberlina site's apparent position in an area of transitional fault density. As more fields exist in the quadrants with higher average density, it may be that the density aggregate from the fields overestimates the fault density in the vicinity of Kimberlina. This would lead to a higher than actual estimate of fault encounter probability.

Fault Density Modeling

Fault density is plotted against specific throw truncation in Figure 10. While it is tempting to see this distribution as exponential given the good fit to the data, low displacement faults are underreported due to the fault mapping resolution limit (Pickering et al. 1995). As a result, the actual fault population is larger than the measured data at the low end of the range. The exponential fit, as good as it is, actually under predicts the fault density at low throw cutoffs.

Alternatively, the throw truncation intervals and range of values fitted was varied to find the largest range that could be well fit linearly. This resulted in a line that lies above the data at low throw cutoff, in accord with the mapping resolution effect. The point of departure of the linear fit from the fault-density data is at a throw cutoff of approximately 20 m (65 ft). This is reasonable as it is slightly lower than the average contour interval of 23 m (76 ft) for the oil and gas field structure maps. Consequently, the linear fit appears more likely to represent the actual fault population in the vicinity of the Kimberlina site, indicating that the fault population follows a power-law distribution. The power law fit also yields higher fault density estimates at low

throw truncations, which makes it more conservative than the exponential fit for estimating leakage risk.

The linear fit also over predicts the fault density at high throw truncations relative to the data according Figure 10. This occurs due to the probability of undersampling of large faults in a given finite mapping area. This typically results in greater downscaling in the throw truncation range than in the fault density range. This causes the data to shift down at the highest throw truncations, the so-called “finite-range effect” of Pickering et al. (1995).

Pickering et al. (1995) presents a correction for this effect. The suggested correction was implemented by including the fault density at the two highest throw truncations in the data set for fitting, adding a constant to each fault density in the data set, and calculating a new linear fit. The constant was varied until the square of the correlation coefficient was maximized. A constant of 0.025 km/km^2 (0.04 mi./mi.^{2}) provided the best fit. The corrected data and fit are shown on Figure 11. The C_d resulting from this correction is 1.16.

A comparison of C_d values from Figures 10 and 11 provides additional support for taking the latter as more accurately representing the fault population than the former. The C_d of 1.43 shown on Figure 10 is larger than values typically reported from field studies, which range from 0.5 to 1.0 (Yielding et al. 1996). Such a value would indicate that the fault network in the Kimberlina area is relatively undeveloped. As mentioned, the faults appear to be primarily due to growth faulting and so perhaps a lower total strain is reasonable. Conversely, most of the mapped faults intersect other faults, suggesting at least moderate development of the fault network. This would tend to support the contention that the C_d on Figure 10 is too large.

The corrected C_d of 1.16 shown on Figure 11 is more commensurate with the reported range and the observed degree of fault network development. Further, as mentioned, lower

values of C_d correlate with a higher density of large offset faults relative to low offset faults. As large offset faults are of more concern for leakage (as discussed below), the lower estimate of C_d is also more conservative with regard to estimating leakage risk.

Throw Interpolation

The throw at one end of a fault segment will typically be different from that at the other end. Some method for estimating the portion of the segment with *d* must be chosen. This method could simply be a linear interpolation between the displacements at the two end points, or some higher order interpolation of displacement along the fault using multiple values. Alternatively, the segment length could simply be bifurcated with each half assigned the throw at nearest end. The simplicity of the latter strategy comes at the cost of error in *F* for a particular *d* given a specific fault, but this error should shrink to a generally small value for a larger fault set. In the case of the current set under consideration, fault densities at each value of d were calculated using both the segment bifurcation and linear interpolation approaches. There was negligible difference in the distribution of *F* resulting from these two methods, suggesting the simpler bifurcation method can be used without concern for larger fault sets.

Fault Encounter Probability

An estimate of the reservoir area swept by carbon dioxide due to the proposed injection can be measured from numerical simulation results. The anticipated CO_2 plume at the Kimberlina site was numerically simulated using the ECO2N equation of state package of TOUGH2 (Pruess and Garcia 2002, Doughty 2010). The model simulated the injection of 250,000 t/yr of CO_2 for four years, then simulated migration and trapping of the plume over the next 46 years. Figure 12 shows CO_2 saturation and saturation above residual saturation at several

time steps in the numerical modeling. Saturation above residual is referred to as the mobile fraction. On Figure 12, zero is no saturation above residual, and one is 100% saturation.

The area within the outer contour on the last frame of Figure 12 is the region swept by CO2 since the start of injection. This area changes little after 30 years, and so is termed the "plume area" for the purposes of analyzing the probability of mobile CO_2 encountering a fault. This definition of the plume area differs from other possible definitions, such as the area swept by dissolved CO_2.

Considering the predominant fault orientation in the vicinity of the Kimberlina site as discussed above, the fault-perpendicular plume dimension measured from Figure 12 is 1.06 km (0.62 mi.), which is equal to 2*k*. Faults with throws that fully offset the caprock overlying a prospective storage reservoir are one particular focus of concern (not that leakage along faults with smaller throws is not possible). The sealing formations over the Vedder have a vertical thickness of approximately 180 m (600 ft). The corrected fault density equation on Figure 11 indicates the average density of faults with this throw truncation is 0.028 km/km^2 (0.046 mi./mi.^{2}). So the probability of the plume resulting from the proposed Kimberlina injection encountering such a fault is 3.2% according to Equation 8.

Conclusions

Storage of carbon dioxide in subsurface reservoirs is one possible means for reducing greenhouse gas emissions. However, the volume of depleted oil and gas fields is insufficient and is likely to be further limited by concerns regarding injecting carbon dioxide into the remaining resource in place. Consequently, if this technological solution is to move forward storage in

brine-filled reservoirs will need to occur. Less is known about these reservoirs than those containing oil and gas because there has been little economic incentive to characterize them.

The possibility of leakage is one of the main concerns regarding carbon dioxide storage, with leakage along faults a particular focus of concern. In order for leakage to occur, encounter of a fault needs to occur first, followed by movement along a fault. Statistics regarding areal fault density are one input to calculating the probability of such encounters. Past findings and formulations regarding fault population statistics can be applied as well to areal fault density. This provides a means to both check areal fault density statistics measured from available fault mapping, and to formulate these statistics for input. This is particularly useful when carrying out leakage risk assessment in the site-screening stage, or in the site evaluation stage, at sites with limited site-specific characterization of faults.

Once the probability of a plume encountering a fault of a particular size is known, some perspective on the probability of leakage along that fault can be gained from its throw and the lithology of the displaced section by calculating the shale-gouge ratio along the fault (Yielding et al. 1996). The probability of a fault plume encounter times the probability of fault leakage once an encounter has occurred comprises the total fault leakage probability. However, this presumes fault encounter and leakage along a fault are independent events. Consequently this approach would not hold in some cases, such as fields with a significant probability of induced seismicity on the faults of interest.

One outcome of the application of the fault-population approach to fault encounter probability assessment is the realization that CO_2 plumes will encounter faults of some size in most geologic sequestration environments because small-offset faults occur at high densities. This does not mean a priori that significant leakage will necessarily occur via these smaller

faults, as evidenced by the persistence of buoyant hydrocarbon deposits frequently, if not typically, occurring in association with faulted terrain. This understanding should shift the consideration of leakage via faults from a more simple concern for plumes encountering faults, to a more detailed assessment of which faults are likely to be of concern, and what happens if the plume encounters those faults.

Acknowledgments

We are grateful to Chris Doughty (LBNL) for sharing the Kimberlina Phase III pilot test simulation results, and to Jeff Wagoner (LLNL) for sharing his expertise regarding the geology of the southern San Joaquin Valley, particularly in the vicinity of the Kimberlina site. We thank Tiemi Onishi for providing an internal review. This said, the authors take full responsibility for the data analysis and conclusions presented. This work was supported in part by the CO_2 Capture Project (CCP) of the Joint Industry Program (JIP), and by Lawrence Berkeley National Laboratory under U.S. Department of Energy Contract No. DE-AC02-05CH11231.

REFERENCES

Ackerman, R. V., R. W. Schlische and M. O. Withjack (2001). The geometric and statistical evolution of normal fault systems: an experimental study of the effects of mechanical layer thickness on scaling laws. Journal of Structural Geology. 23, 1803-1819.

Bloch, R. B. (1986). Ramp-style deposition of Oligocene marine Vedder formation, San JoaquinValley. California, AAPG Bulletin. 70, 4.

Cowie, P. A., D. Sornette and C. Vanneste (1995). Multifractal scaling properties of a growing fault population. Geophysical Journal International. 122, 457-469.

Doughty, C. (2010). Investigation of CO_2 plume behavior for a large-scale pilot test of geologic carbon storage in a saline formation. LBNL-2243E. Transport in Porous Media: Special Issue on Geologic Carbon Storage, published online, DOI 10.1007/s11242-009-9396-z, Springer.

Energy Information Agency (EIA) (2009). Emissions of greenhouse gases report. DOE/EIA-0573(2008). Released 3 December 2009, revised 8 December 2009. http://www.eia.doe.gov/oiaf/1605/ggrpt/carbon.html.

Graham, S. A. and L. A. Williams (1985). Tectonic, depositional, and diagenetic history of Monterey Formation (Miocene), Central San Joaquin Basin, California. AAPG Bulletin. 69: 385-411.

Jordan, P.D., C.M. Oldenburg, and J.P. Nicot (2011). Calculating the probability of injected carbon dioxide plumes encountering faults. Submitted to the International Journal of Greenhouse Gas Control.

McPherson, B. A. (1978). Sedimentation and trapping mechanisms in Upper Miocene Stevens and older turbidite fans of the southeastern San Joaquin Valley, California. AAPG Bulletin. 62, 2243-2274.

National Energy Technology Laboratory (NETL) (2009). West Coast Regional Sequestration Partnership – development phase. 4 p. http://www.netl.doe.gov/publications/factsheets/project/Proj596.pdf accessed on June 9, 2009.

Pickering, G., J. M. Bull and D.J. Anderson (1995). Sampling power-law distributions. Tectonophysics. 248, 1-20.

Wagoner, J. (2009). 3D Geologic Modeling of the Southern San Joaquin Basin for the Westcarb Kimberlina Demonstration Project- A Status Report. Lawrence Livermore National Laboratory, LLNL-TR-410813.

Watterson, J., J. J. Walsh, P. A. Gillispie and S. Eaton (1996). Scaling systematics of fault sizes on a large-scale range fault map. Journal of Structural Geology. 18, 199 – 214.

Yielding, G., B. Freeman, and D. T. Needham (1996). Quantitative fault seal prediction. AAPG Bulletin. 81, 897 – 917.

Zhang, Y., C.M. Oldenburg, and S. Finsterle (2010). Percolation-theory and fuzzy rule-based probability estimation of fault leakage at geologic carbon sequestration sites. LBNL-2172E. Environmental Earth Sciences, 59 (7), 144–159; published online, DOI: 10.1007/s12665-009-0131-4.

FIGURE CAPTIONS

Figure 1. Location of the Kimberlina Phase III pilot test in the San Joaquin Basin in California (modified from Sheirer 2007).

Figure 2. Oil and gas fields in the vicinity of the Kimberlina site. The Kimberlina site is at the star. North is up. (modified from DOGGR 1998)

Figure 3. Structure map of Calders Corner oil field modified from DOGGR (1998). Italic values are interpolated throws in feet. Large values are interpolated elevations of fault-block corners in feet relative to sea level. Dashed line is boundary of coverage area. The Stevens is a productive zone in the Fruitvale, which is shown on Figure 7.

Figure 4. Percent of fault length occurring in 10° strike intervals in oil and gas fields centered within 24 km (15 mi.) of the Kimberlina site.

Figure 5. Percent of fault length occurring in 10° strike intervals in oil and gas fields centered within 16 km (10 mi.) of the Kimberlina site.

Figure 6. Percent of fault length occurring in 10° strike intervals in oil and gas fields centered between 16 km (10 mi.) and 24 km (15 mi.) of the Kimberlina site.

Figure 7. Generalized section for the southeastern San Joaquin basin (DOGGR 1998).

Figure 8. Fault density for individual oil and gas fields plotted against the vertical distance from the structural map horizon to the Vedder Formation. Positive values indicate the Vedder is deeper than the section. Symbol area is proportional to field structure map area.

Figure 9. Approximate direction and distance to each field. Relative field size and fault density represented by circle diameter. Empty circles are fields without faults.

Figure 10. Fault density versus throw truncation aggregated from the structure maps for the oil and gas fields shown on Figure 2. Data are shown as closed boxes. Heavy line is linear fit to selected data (see text). Lighter line is exponential fit to all data. Dashed lines are extrapolated from the fit lines.

Figure 11. Fault density versus throw truncation aggregated from the structure maps for the oil and gas fields shown on Figure 2. Data are shown as open boxes. Lighter line is linear fit to selected data (see text). Corrected data are shown as closed boxes. Heavy line is linear fit to selected corrected data. Dashed lines are extrapolated from the fit lines.

Figure 12. Numerically simulated total CO_2 saturation and saturation in excess of residual. Total saturation is shown by contours. Saturation in excess of residual is shown by tints. Note the tints for saturation in excess of residual are defined on a log scale. Coordinates are in meters. North is up. (Courtesy of Christine Doughty, LBNL).

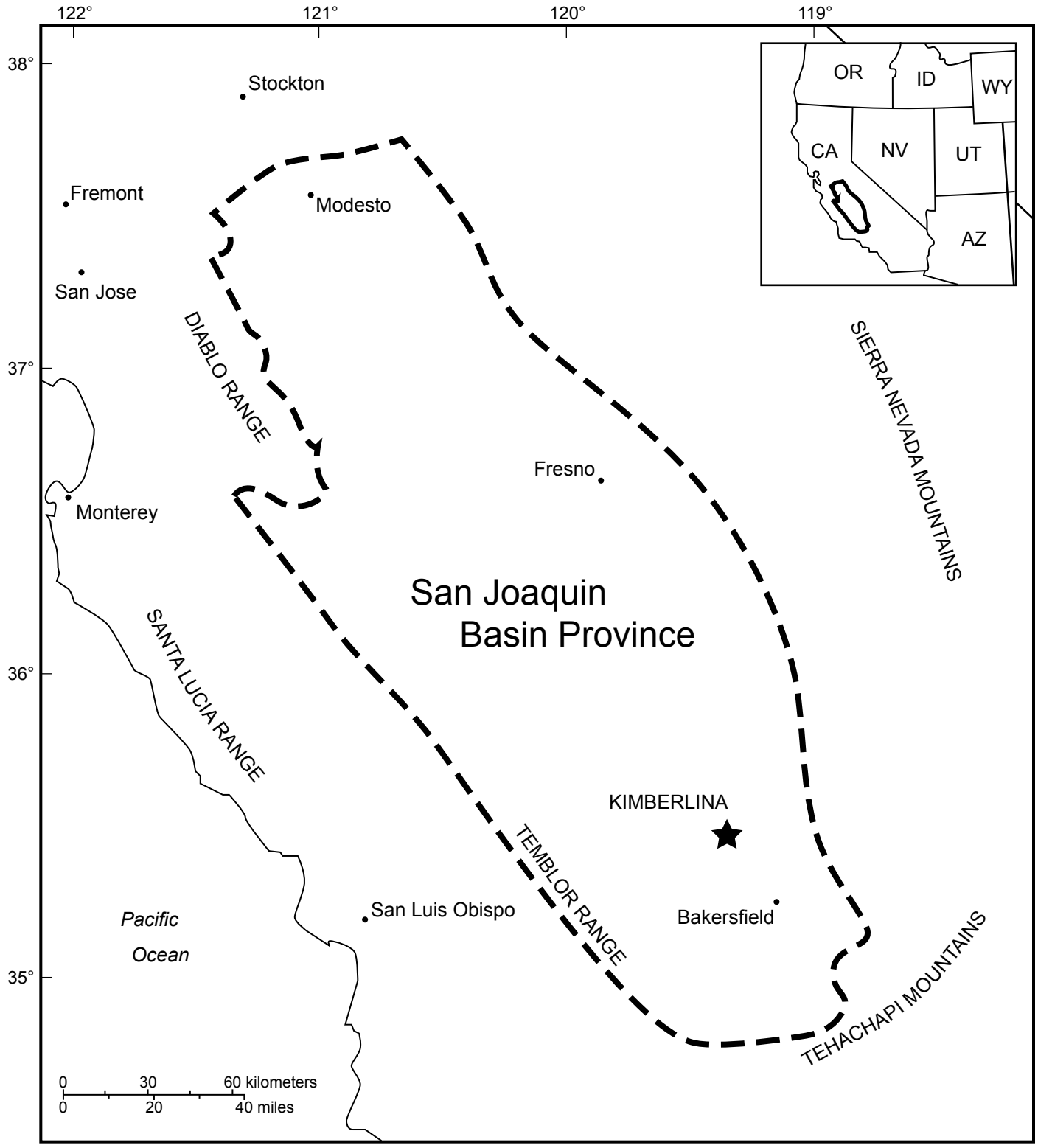
122°
121°
120°
119°
38°
37°
36°
35°
Stockton
Fremont
Modesto
San Jose
Monterey
Fresno
KIMBERLINA
San Luis Obispo
Bakersfield
Pacific
Ocean
DIABLO RANGE
SIERRA NEVADA MOUNTAINS
SANTA LUCIA RANGE
TEMBLOR RANGE
TEHACHAPI MOUNTAINS
San Joaquin
Basin Province
OR
ID
WY
CA
NV
UT
AZ
0
30
60 kilometers
0
20
40 miles

Figure 1

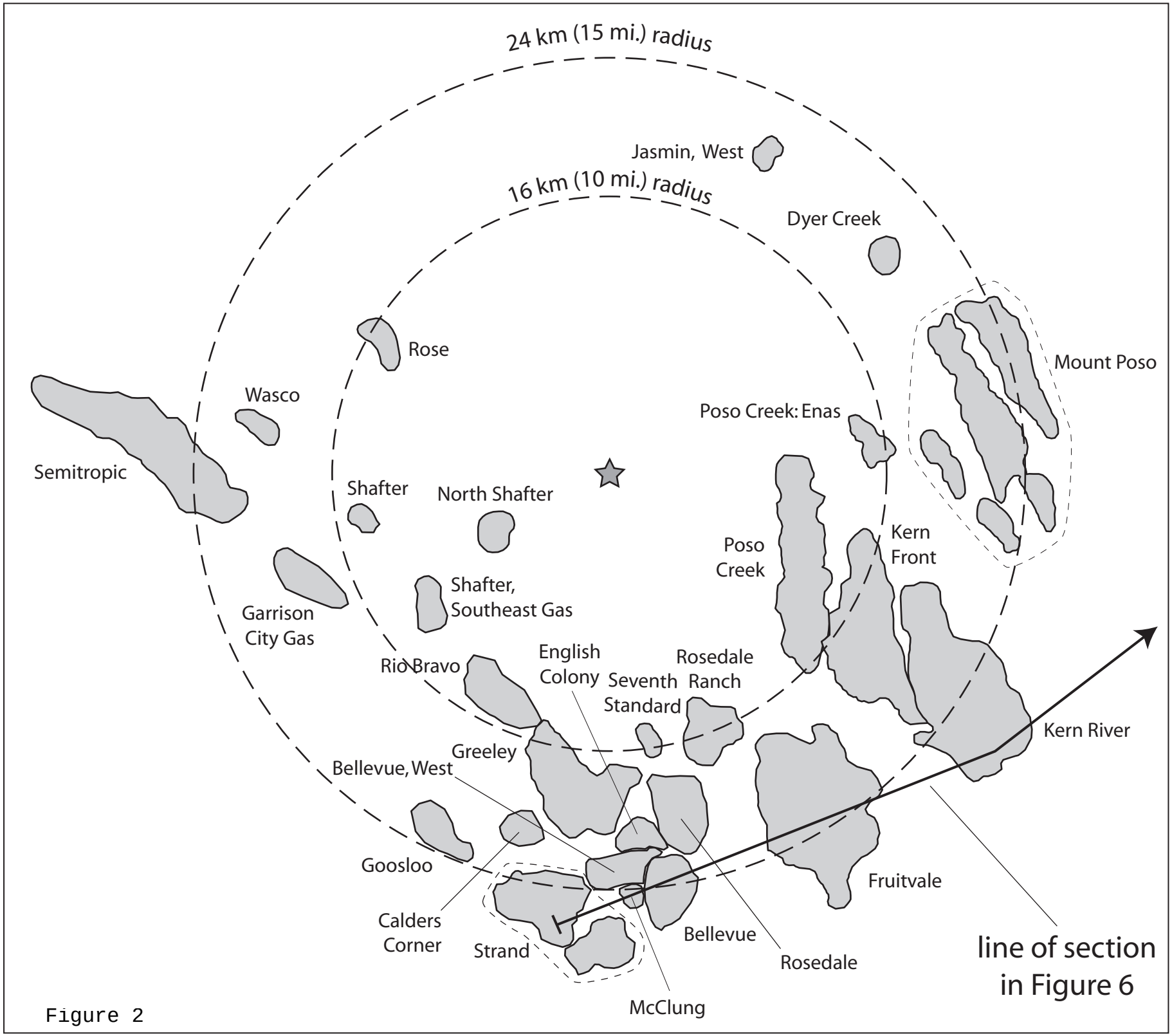
24 km (15 mi.) radius
16 km (10 mi.) radius
Jasmin, West
Dyer Creek
Rose
Mount Poso
Wasco
Poso Creek: Enas
Semitropic
Shafter
North Shafter
Poso
Creek
Kern
Front
Shafter,
Southeast Gas
Garrison
City Gas
English
Colony
Rosedale
Ranch
Rio Bravo
Seventh
Standard
Kern River
Greeley
Bellevue, West
Goosloo
Fruitvale
Calders
Corner
Strand
Bellevue
Rosedale
line of section
in Figure 6
McClung

Figure 2

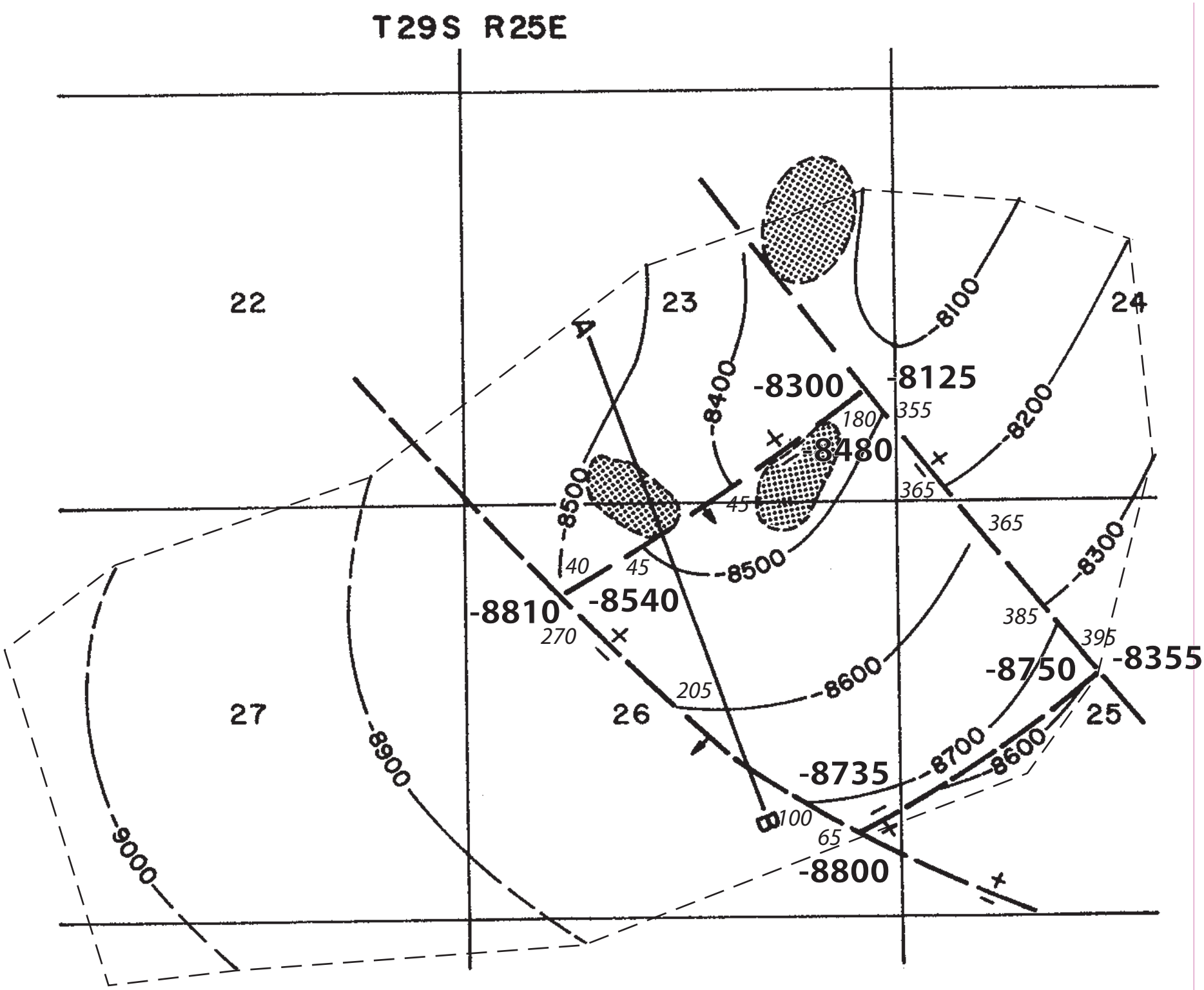

CONTOURS ON TOP OF STEVENS

Figure 3

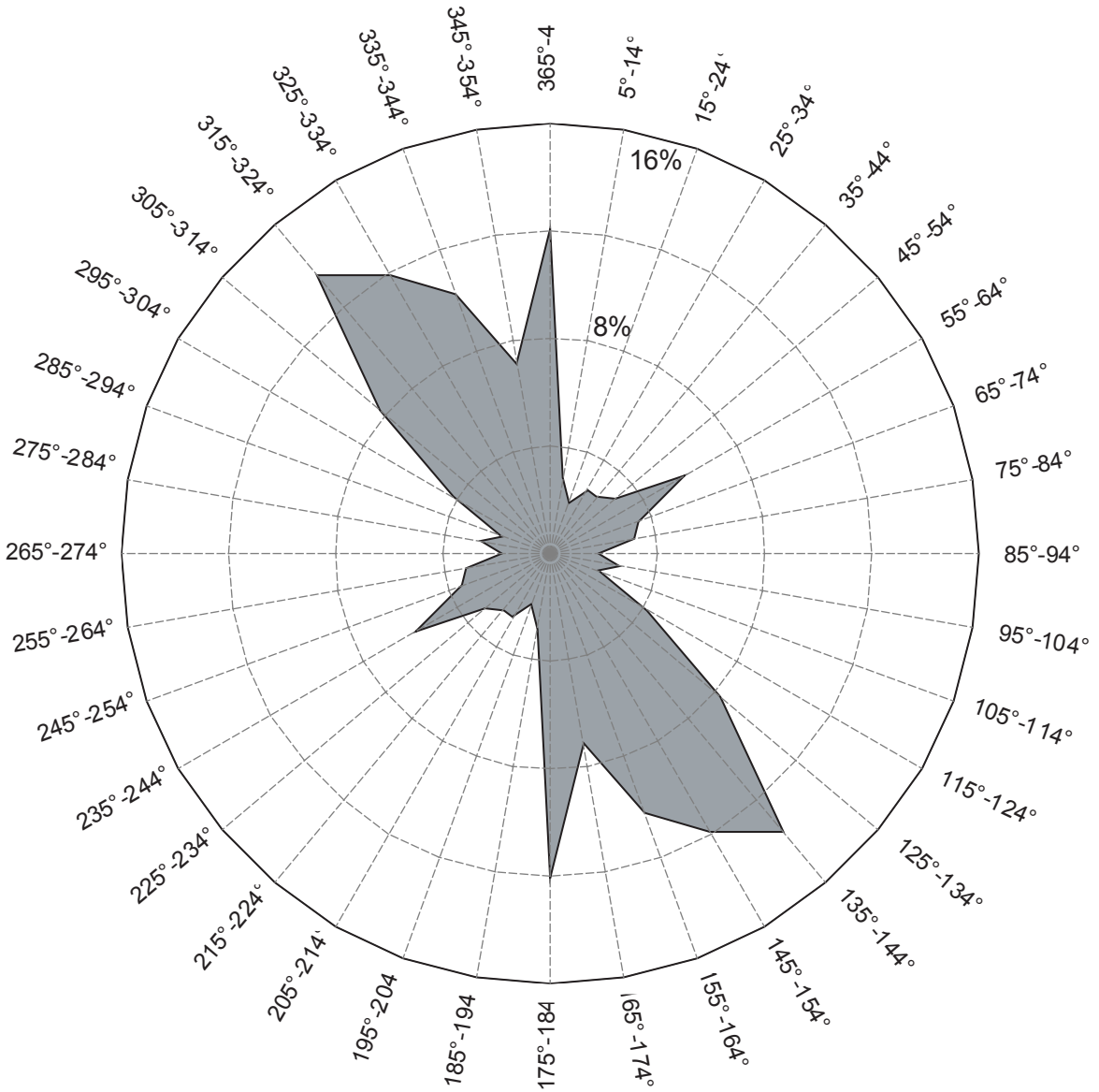

total fault length: 465 km (289 mi.)

Figure 4

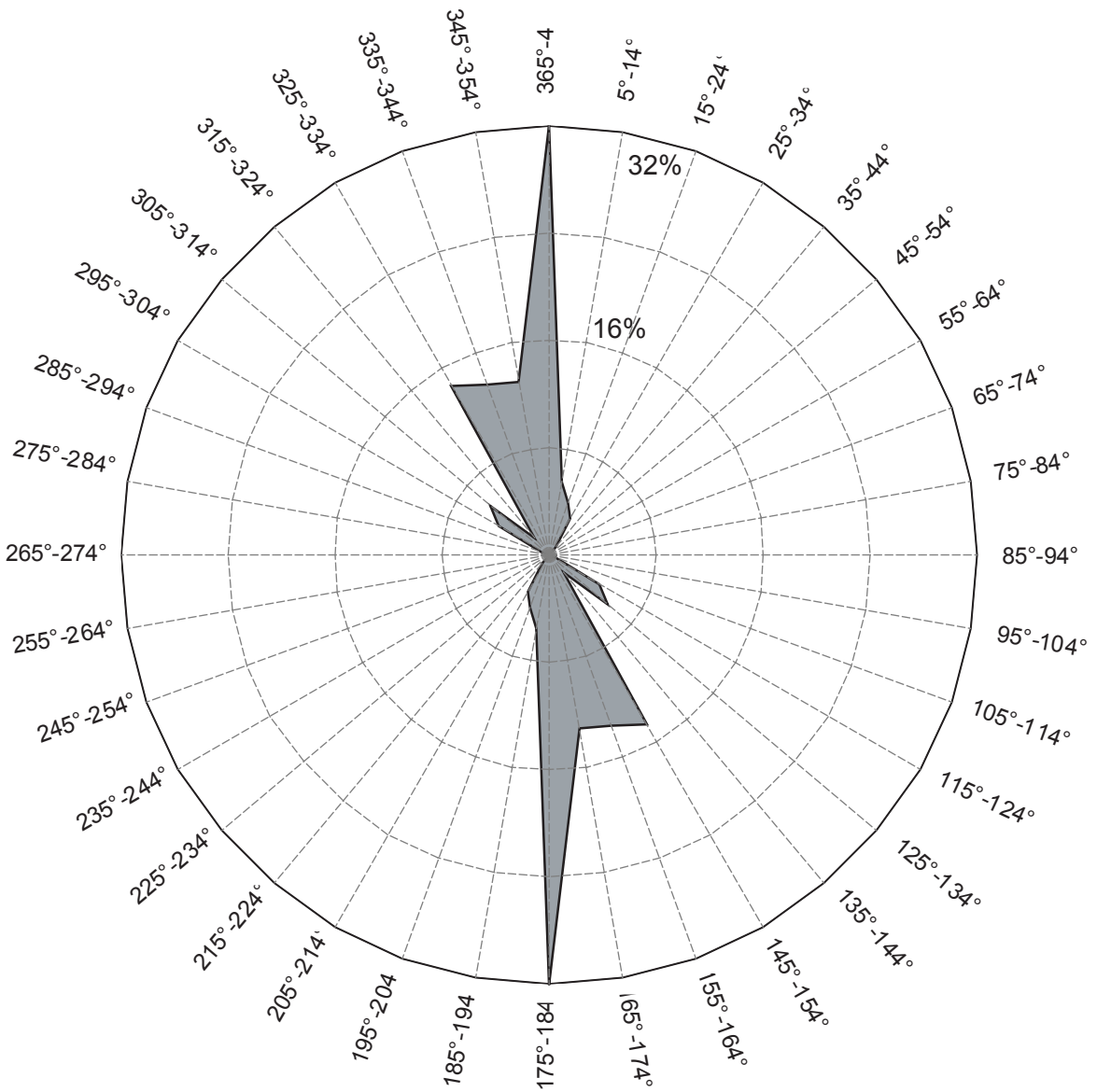

total fault length: 80 km (50 mi.)

Figure 5

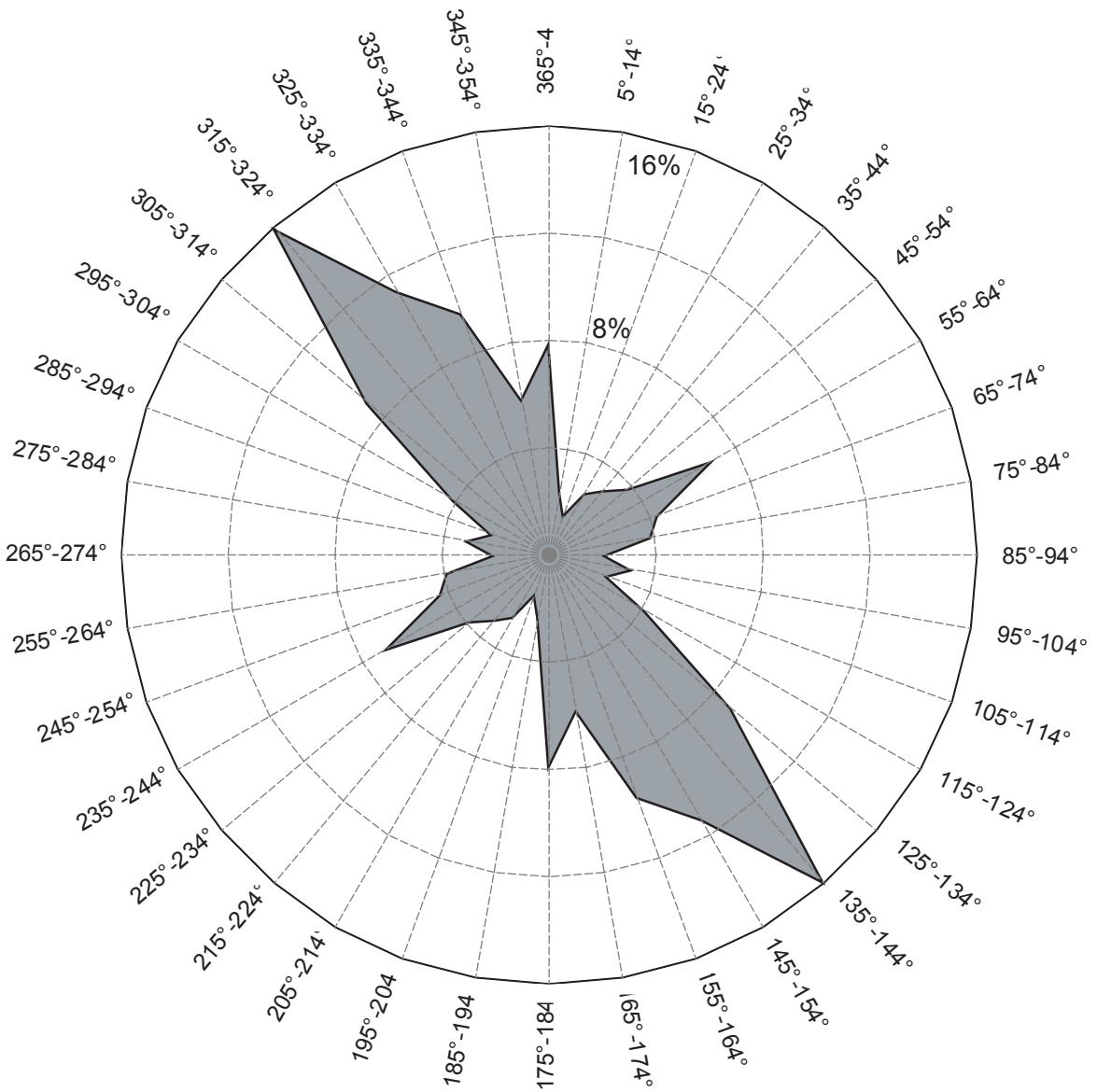

total fault length: 384 km (239 mi.)

Figure 6

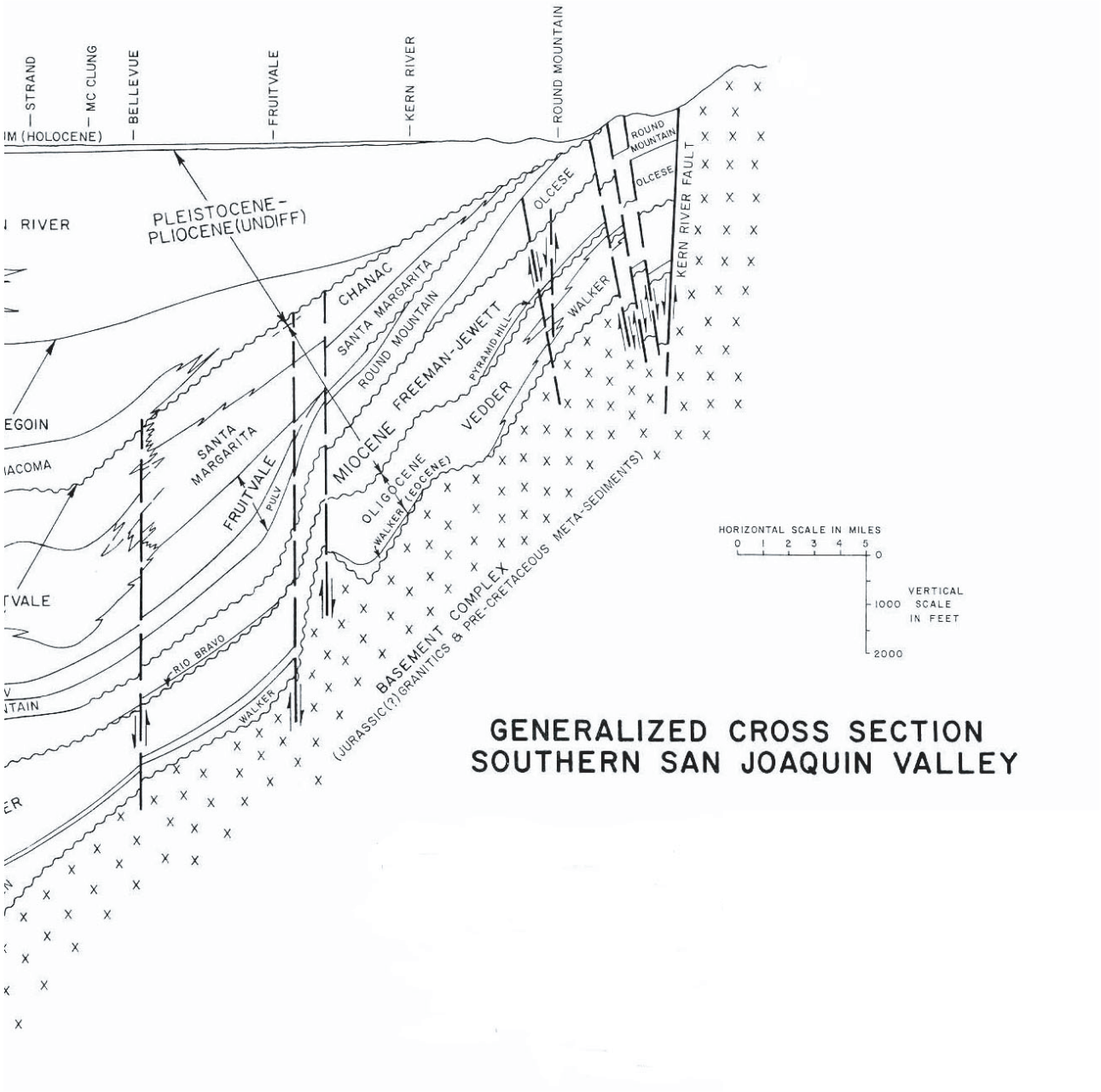
STRAND
MC CLUNG
BELLEVUE
FRUITVALE
KERN RIVER
ROUND MOUNTAIN
IM (HOLOCENE)
PLEISTOCENE-
PLIOCENE(UNDIFF)
ROUND MOUNTAIN
OLCESE
OLCESE
KERN RIVER FAULT
CHANAC
SANTA MARGARITA
ROUND MOUNTAIN
FREEMAN-JEWETT
PYRAMID HILL
WALKER
VEDDER
SANTA MARGARITA
FRUITVALE
POLV
MIOCENE
OLIGOCENE
WALKER (EOCENE)
RIO BRAVO
WALKER
BASEMENT COMPLEX
(JURASSIC(?) GRANITICS & PRE-CRETACEOUS META-SEDIMENTS)
HORIZONTAL SCALE IN MILES
0 1 2 3 4 5
0
1000
2000
VERTICAL SCALE IN FEET
GENERALIZED CROSS SECTION
SOUTHERN SAN JOAQUIN VALLEY

Figure 7

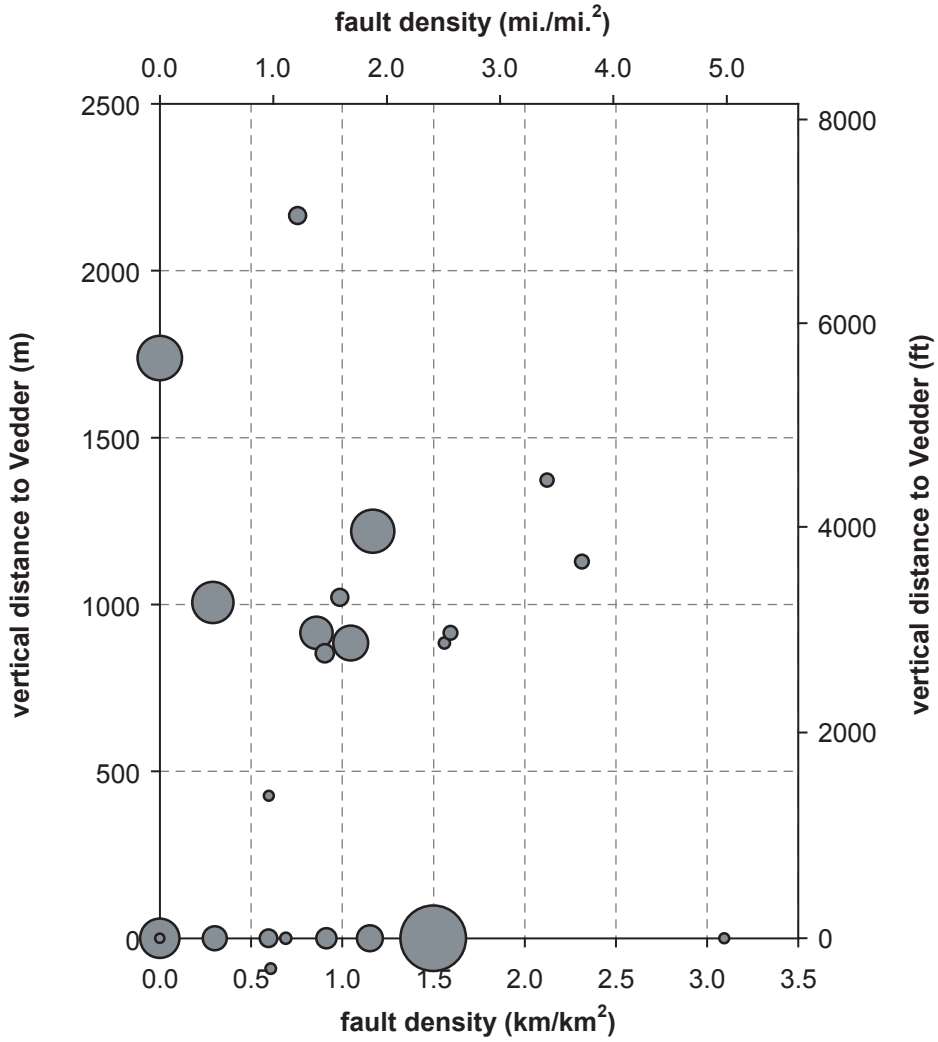
fault density (mi./mi.^{2})
0.0
1.0
2.0
3.0
4.0
5.0
2500
2000
1500
1000
500
0
8000
6000
4000
2000
0
vertical distance to Vedder (m)
vertical distance to Vedder (ft)
0.0
0.5
1.0
1.5
2.0
2.5
3.0
3.5
fault density (km/km^2)

Figure 8

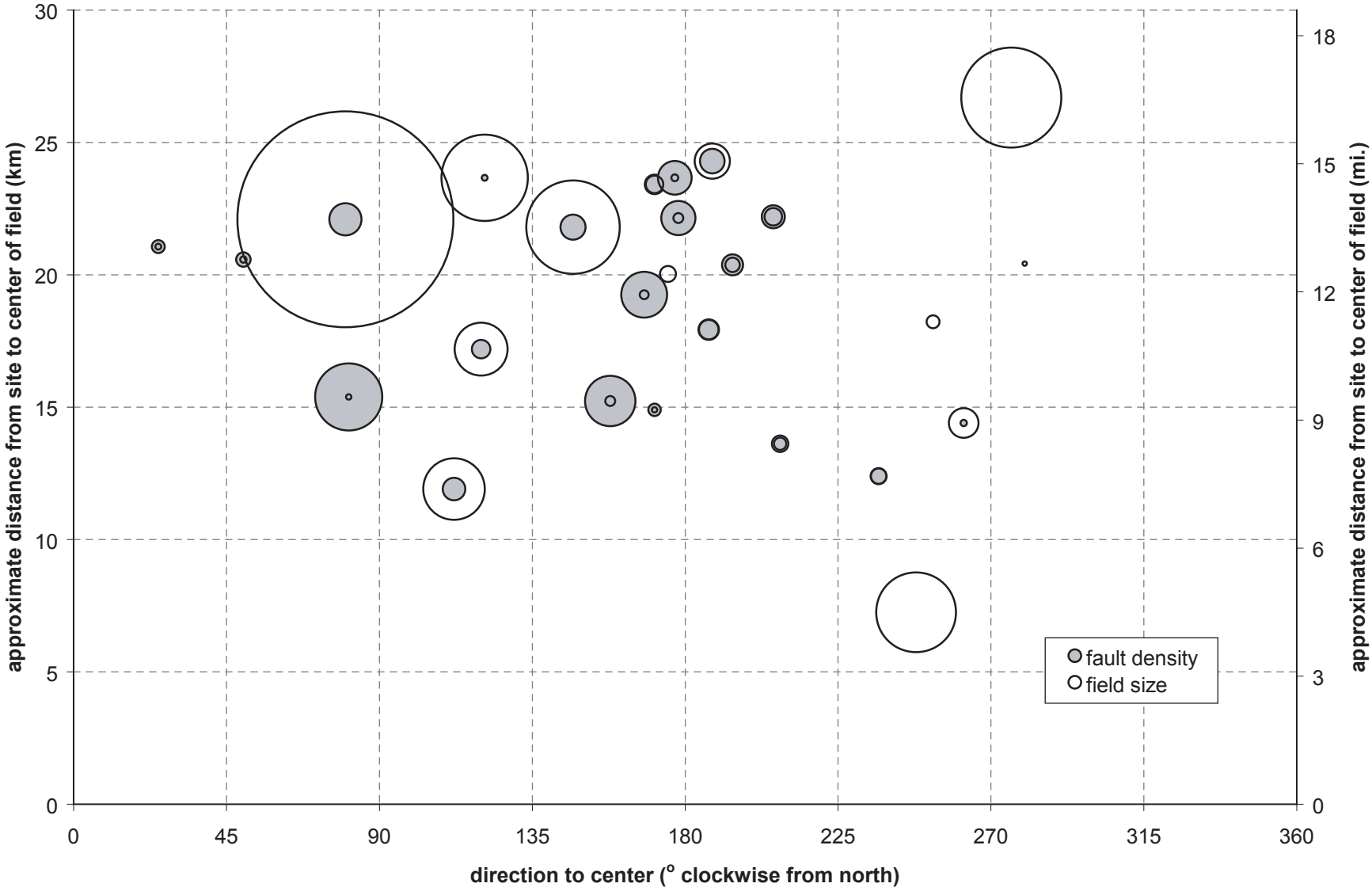
approximate distance from site to center of field (km)
approximate distance from site to center of field (mi.)
direction to center (° clockwise from north)
0
45
90
135
180
225
270
315
360
5
10
15
20
25
30
3
6
9
12
18
fault density
field size

Figure 9

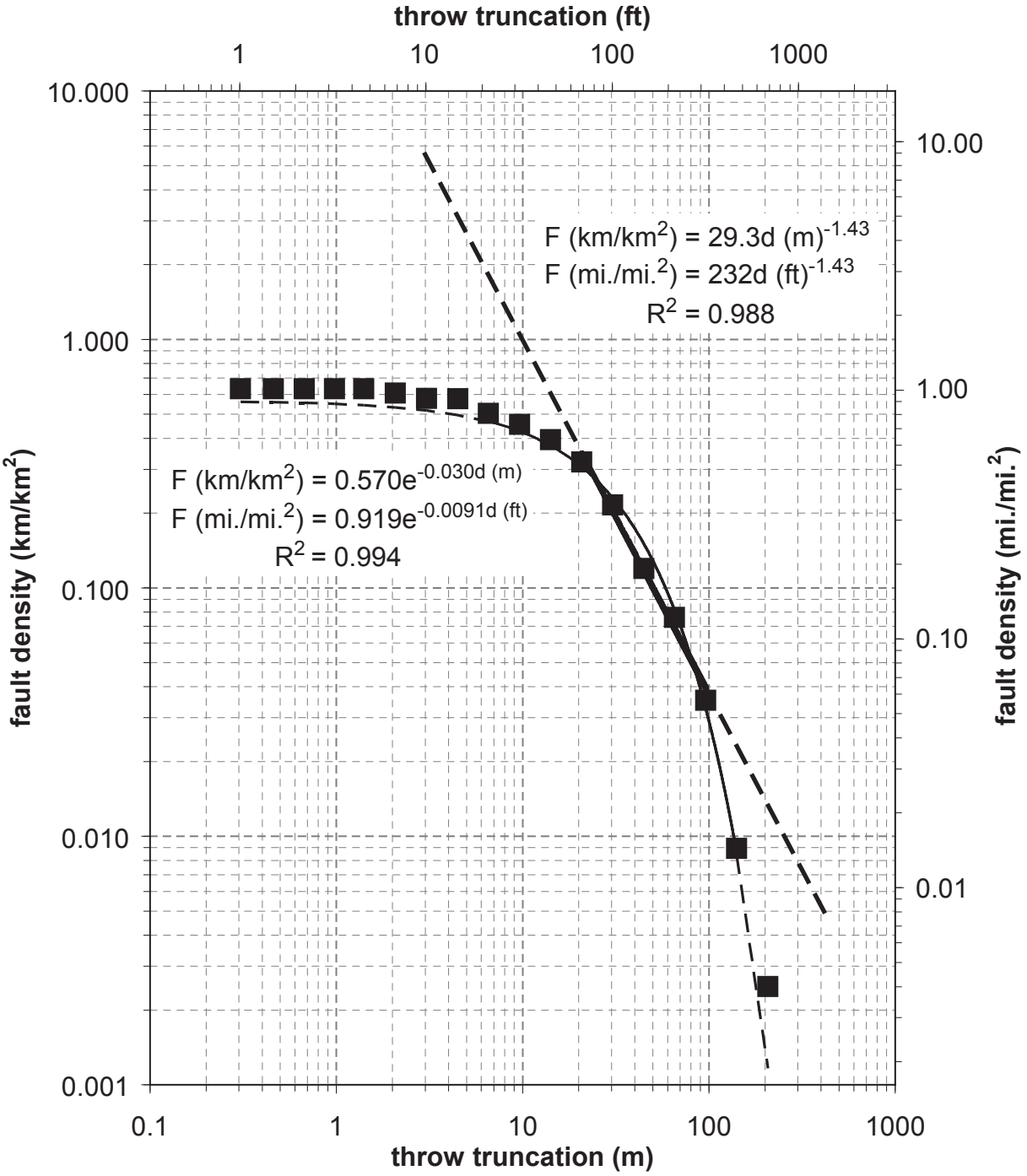
throw truncation (ft)
1
10
100
1000
10.000
1.000
0.100
0.010
0.001
10.00
1.00
0.10
0.01
F (km/km^2) = 29.3d (m)$^{-1.43}$
F (mi./mi.^{2}) = 232d (ft)$^{-1.43}$
R^2 = 0.988
F (km/km^2) = 0.570e$^{-0.030d\ (m)}$
F (mi./mi.^{2}) = 0.919e$^{-0.0091d\ (ft)}$
R^2 = 0.994
fault density (km/km^2)
fault density (mi./mi.^{2})
0.1
1
10
100
1000
throw truncation (m)

Figure 10

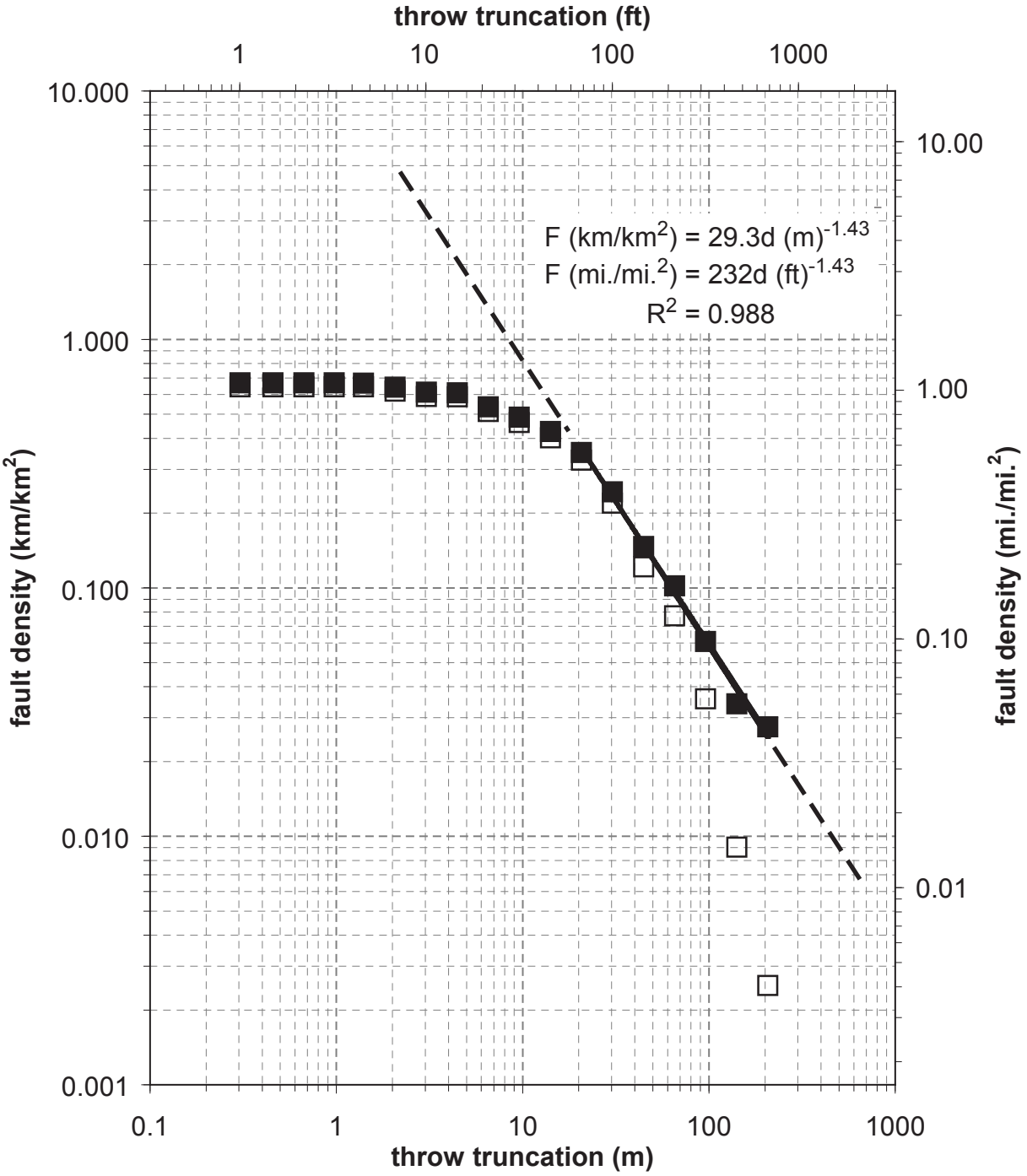
throw truncation (ft)
1
10
100
1000
10.000
1.000
0.100
0.010
0.001
10.00
1.00
0.10
0.01
F (km/km^2) = 29.3d (m)$^{-1.43}$
F (mi./mi.^{2}) = 232d (ft)$^{-1.43}$
R^2 = 0.988
fault density (km/km^2)
fault density (mi./mi.^{2})
0.1
1
10
100
1000
throw truncation (m)

Figure 11

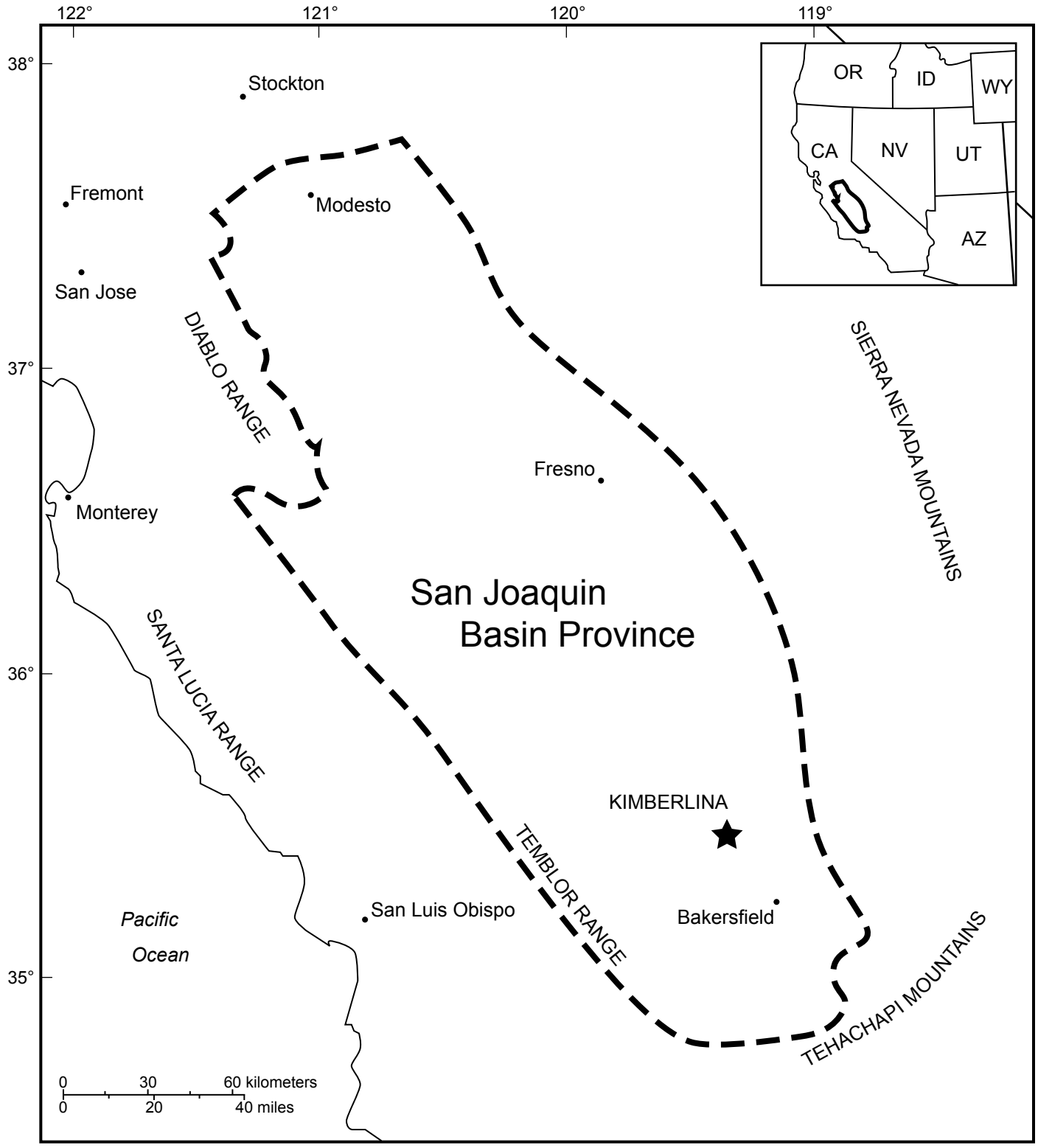
122°
121°
120°
119°
38°
37°
36°
35°
Stockton
Fremont
Modesto
San Jose
Monterey
Fresno
KIMBERLINA
San Luis Obispo
Bakersfield
Pacific
Ocean
DIABLO RANGE
SIERRA NEVADA MOUNTAINS
SANTA LUCIA RANGE
TEMBLOR RANGE
TEHACHAPI MOUNTAINS
San Joaquin
Basin Province
OR
ID
WY
CA
NV
UT
AZ
0 30 60 kilometers
0 20 40 miles

Figure 12

Appendix 1

field	fault		apparent vertical offset		length (ft)	strike	note
	number	segment	start	end			
Bellevue	1	1	35	65	870	9	
Bellevue	1	2	65	110	1038	8	
Bellevue	1	3	110	165	732	6	
Bellevue	1	4	165	240	534	8	
Bellevue	1	5	240	295	656	6	
Bellevue	1	6	295	345	824	10	
Bellevue	1	7	345	380	778	8	
Bellevue	1	8	380	395	763	8	
Bellevue	1	9	395	330	763	9	
Bellevue	1	10	330	270	961	9	
Bellevue	1	11	330	320	1083	4	
Bellevue	1	12	320	255	1190	4	
Bellevue	1	13	255	165	870	0	
Bellevue	1	14	165	125	4059	179	
Bellevue	2	1	20	20	748	132	
Bellevue	2	2	20	30	2243	123	
Bellevue	2	3	30	75	626	123	
Bellevue	2	4	75	75	794	117	
Bellevue	2	5	75	60	977	114	
Bellevue	2	6	60	75	977	115	
Bellevue	2	7	75	60	687	108	
Bellevue	3	1	10	40	1862	140	
Bellevue	3	2	40	45	1877	139	
Bellevue	3	3	45	45	2960	141	
Bellevue	3	4	45	15	1801	140	
Bellevue West	1	1			2071	142	
Bellevue West	1	2			975	143	
Bellevue West	2	1	5	5	457	122	
Bellevue West	2	2	5	10	802	120	
Bellevue West	2	3	10	5	630	117	
Bellevue West	2	4	5	10	640	118	
Bellevue West	2	5	10	10	538	112	
Bellevue West	2	6	10	10	518	110	
Bellevue West	3	1	15	15	711	134	
Bellevue West	3	2	15	5	995	134	
Bellevue West	3	3	5	5	670	133	
Bellevue West	3	4	10	15	721	133	
Bellevue West	3	5	15	15	589	131	
Bellevue West	3	6	15	10	335	133	
Bellevue West	3	7	45	30	294	133	
Bellevue West	3	8	30	25	447	131	
Bellevue West	3	9	25	25	447	129	
Bellevue West	3	10	25	20	284	131	
Bellevue West	4	1	20	15	1472	70	
Bellevue West	4	2	15	10	762	68	
Bellevue West	4	3	10	15	741	70	
Bellevue West	4	4	15	10	914	68	
Bellevue West	4	5	25	20	599	67	

field	fault		apparent vertical offset		length (ft)	strike	note
	number	segment	start	end			
Bellevue West	4	6	85	65	883	67	
Bellevue West	4	7	65	0	1432	64	
Bellevue West	4	8	0	25	843	61	
Bellevue West	4	9	25	35	853	58	
Bellevue West	5	1	15	15	274	47	
Bellevue West	5	2	15	10	467	49	
Bellevue West	5	3	10	15	538	46	
Bellevue West	5	4	15	15	467	44	
Bellevue West	5	5	15	30	650	40	
Bellevue West	5	6	30	0	437	38	
Bellevue West	5	7	0	30	437	38	
Bellevue West	5	8	30		619	36	
Bellevue West	5	9			416	33	
Bellevue West	6	1	35	60	1371	141	
Bellevue West	6	2	60	75	762	143	
Bellevue West	6	3	75	15	640	141	
Bellevue West	7	1	65	40	1310	140	
Bellevue West	7	2	40	15	1706	140	
Bellevue West	7	3	30	30	213	140	
Calders Corner	1	1			3727	136	
Calders Corner	1	2	270	205	2065	134	
Calders Corner	1	3	205	100	2034	124	
Calders Corner	1	4	100	65	714	121	
Calders Corner	1	5			2423	114	
Calders Corner	2	1			3339	142	
Calders Corner	2	2	355	365	1600	142	
Calders Corner	2	3	365	365	699	142	
Calders Corner	2	4	365	385	1227	139	
Calders Corner	2	5	385	390	1072	140	
Calders Corner	2	6			901	141	
Calders Corner	3	1	40	45	1211	60	
Calders Corner	3	2	45	45	1367	56	
Calders Corner	3	3	45	180	2019	55	
Calders Corner	4	1			1103	61	
Calders Corner	4	2			2485	55	
Dyer Creek	1	1	155	155	9141	143	
Fruitvale	1	1			3400	155	
Fruitvale	1	2			680	166	
Fruitvale	1	3	35	15	3360	164	
Fruitvale	1	4	10	10	560	170	
Fruitvale	1	5	45	25	480	169	
Fruitvale	1	6	30	40	3000	168	
Fruitvale	2	1			2240	147	
Fruitvale	2	2			1360	146	
Fruitvale	3	1	90	90	1520	151	
Fruitvale	3	2	95	85	3440	145	
Fruitvale	4	1	95	60	3680	147	
Fruitvale	5	1	55	50	1240	108	

field	fault		apparent vertical offset		length (ft)	strike	note
	number	segment	start	end			
Fruitvale	5	2	50	35	3040	110	
Fruitvale	6	1	50	35	6160	143	
Fruitvale	7	1	0	55	3560	123	
Fruitvale	7	2	40	45	1960	130	
Fruitvale	7	3	10	0	1800	130	
Fruitvale	7	4	0	5	4480	132	
Fruitvale	7	5	5	5	1080	132	
Fruitvale	7	6	20	20	2960	134	
Fruitvale	7	7	20	20	1840	141	
Fruitvale	7	8	20	20	1880	155	
Fruitvale	8	1	35	15	2560	134	
Fruitvale	8	2	30	30	4280	134	
Fruitvale	8	3	30	0	5320	134	
Fruitvale	9	1			1680	164	
Fruitvale	9	2	0	0	2840	164	
Fruitvale	9	3	0	5	2520	164	
Fruitvale	9	4	5	10	2280	163	
Fruitvale	9	5	10	0	2120	162	
Fruitvale	9	6	0	0	3400	162	
Fruitvale	9	7	0	0	2840	162	
Fruitvale	10	1	10	10	4360	96	
Fruitvale	11	1			1040	76	
Fruitvale	12	1			2320	89	
Fruitvale	12	2			1760	86	
Fruitvale	12	3			480	87	
Fruitvale	12	4			960	83	
Fruitvale	13	1			3720	77	
Fruitvale	14	1	35	35	640	73	
Fruitvale	14	2	35	40	1160	73	
Fruitvale	14	3	40	30	1000	73	
Fruitvale	14	4	30	35	1240	73	
Fruitvale	14	5	35	25	880	73	
Fruitvale	15	1	35	35	920	70	
Fruitvale	15	2	120	40	1920	72	
Fruitvale	15	3	40	5	2880	71	
Fruitvale	16	1	115	115	680	70	
Fruitvale	16	2	0	15	1440	63	
Fruitvale	16	3	50	40	1360	65	
Fruitvale	16	4	35	35	1400	64	
Fruitvale	16	5	35	25	1480	64	
Fruitvale	16	6	25	5	1400	64	
Fruitvale	16	7	5	0	1160	65	
Fruitvale	17	1			3000	55	
Fruitvale	17	2	45	50	1600	56	
Fruitvale	17	3	50	55	920	53	
Fruitvale	17	4	15	15	1160	64	
Fruitvale	17	5	35	25	1600	64	
Fruitvale	17	6	25	20	800	58	

field	fault		apparent vertical offset		length (ft)	strike	note
	number	segment	start	end			
Fruitvale	17	7	60	55	1120	60	
Fruitvale	17	8	55	30	1360	60	
Fruitvale	17	9	30	5	1400	58	
Fruitvale	17	10	40	55	1040	59	
Fruitvale	18	1	15	0	3840	58	
Fruitvale	18	2	0	20	2200	60	
Fruitvale	18	3	20	25	1120	60	
Fruitvale	18	4	25	0	1200	63	
Fruitvale	18	5	0	10	1000	65	
Fruitvale	19	1			2840	54	
Fruitvale	19	2	55	55	1600	54	
Fruitvale	19	3	55	50	840	54	
Fruitvale	19	4	50	50	960	54	
Fruitvale	19	5	50	80	920	54	
Fruitvale	19	6	45	55	1120	55	
Fruitvale	19	7	55	60	1640	54	
Fruitvale	19	8	60	50	1240	53	
Fruitvale	19	9	50	40	720	55	
Fruitvale	19	10	40	0	960	53	
Fruitvale	20	1			3240	72	
Fruitvale	20	2	135	100	1280	72	
Fruitvale	20	3	100	60	1240	73	
Fruitvale	20	4	60	15	1560	72	
Fruitvale	20	5	15	0	1280	73	
Fruitvale	20	6	0	0	1000	70	
Fruitvale	21	1	0	5	920	41	
Fruitvale	21	2	5	0	1200	40	
Fruitvale	21	3	0	0	1000	39	
Fruitvale	22	1			1200	0	
Fruitvale	22	2	35	35	2080	3	
Fruitvale	22	4	35	5	1400	2	
Fruitvale	22	5	5	0	1160	3	
Fruitvale	22	6	0	0	560	3	
Fruitvale	23	1	0	45	480	38	
Fruitvale	23	2	45	65	1240	35	
Fruitvale	23	3	65	20	2560	36	
Fruitvale	23	4			2200	35	
Fruitvale	24	1	0	5	160	30	
Fruitvale	24	2	5	20	960	30	
Fruitvale	24	3	20	35	1040	30	
Fruitvale	24	4	35	70	1280	31	
Fruitvale	25	1			2480	10	
Fruitvale	25	2	235	250	1040	8	
Fruitvale	25	3	125	110	2720	0	
Fruitvale	25	4	180	120	1760	0	
Fruitvale	25	5	120	105	1280	0	
Fruitvale	25	6	105	85	2160	0	
Fruitvale	25	7	65	10	3120	0	

field	fault		apparent vertical offset		length (ft)	strike	note
	number	segment	start	end			
Fruitvale	25	8	0	0	2080	169	
Fruitvale	26	1	125	85	1440	24	
Fruitvale	26	2	855	120	1480	28	
Fruitvale	26	3	120	165	1360	27	
Fruitvale	26	4			1920	28	
Goosloo	1	1			6065	140	
Goosloo	1	2	145	105	1542	136	
Goosloo	1	3	105	135	1897	137	
Goosloo	1	4	135	150	1042	136	
Goosloo	1	5	50	90	1230	134	
Goosloo	1	6	90	140	1938	133	
Goosloo	1	7	140	175	2147	137	
Goosloo	1	8			1167	141	
Goosloo	1	9			2960	164	
Goosloo	2	1			1459	129	
Goosloo	2	2			1396	127	
Goosloo	2	3	40	20	1897	125	
Goosloo	2	4	60	30	2605	125	
Goosloo	2	5	0	15	2814	128	
Goosloo	2	6	25	20	1605	131	
Goosloo	2	7			1459	135	
Goosloo	3	1	40	100	2647	25	
Greeley	1	1			4284	146	right lateral
Greeley	1	2	80	130	1419	148	right lateral
Greeley	1	3	130	90	928	144	right lateral
Greeley	1	4	90	70	682	145	right lateral
Greeley	1	5	70	50	2756	144	right lateral
Greeley	1	6	50	40	1555	143	right lateral
Greeley	1	7	40	100	3465	143	right lateral
Greeley	1	8			12061	143	right lateral
Greeley	2	1			3274	24	
Greeley	2	2			2565	14	
Greeley	2	3			2838	3	
Jasmin, West	1	1			1200	162	
Jasmin, West	1	2	75	80	1706	162	
Jasmin, West	1	3	80	70	1020	162	
Jasmin, West	1	4	70	65	1191	162	
Jasmin, West	1	5	65	70	1309	162	
Jasmin, West	1	6			614	162	
Kern Front	1	1			4718	133	
Kern Front	1	2			1377	141	
Kern Front	1	3			1722	153	
Kern Front	1	4			3030	164	
Kern Front	1	5			3857	176	
Kern Front	1	6			5751	1	
Kern Front	1	7	95	70	2720	14	
Kern Front	1	8	70	50	1240	29	
Kern Front	1	9	50	20	1240	28	

field	fault		apparent vertical offset		length (ft)	strike	note
	number	segment	start	end			
Kern Front	1	10	20	0	1894	39	
Kern Front	2	1	0	10	895	32	
Kern Front	2	2	10	20	1377	37	
Kern Front	2	3	20	30	2101	43	
Kern Front	3	1			2824	3	
Kern Front	3	2	40	10	2789	179	
Kern Front	3	3	10	30	2204	172	
Kern Front	3	4	30	0	1791	159	
Kern Front	4	1	0	25	826	59	
Kern Front	4	2	25	0	689	60	
Kern Front	5	1			2169	31	
Kern Front	5	2	30	0	1653	28	
Kern Front	5	3	0	30	2307	20	
Kern Front	5	4	30	40	1377	34	
Kern Front	5	5	40	20	1722	27	
Kern Front	5	6	20	0	895	19	
Kern Front	6	1			2479	43	
Kern Front	6	2	85	120	1756	52	
Kern Front	6	3	120	120	1102	36	
Kern Front	6	4	120	70	1756	26	
Kern Front	6	5	70	20	2893	28	
Kern Front	6	6	20	0	1963	48	
Kern Front	7	1	0	5	1997	50	
Kern Front	7	2	5	5	1515	42	
Kern Front	7	3	5	5	1653	43	
Kern Front	7	4	5	0	1240	51	
Kern Front	8	1			2238	29	
Kern Front	8	2			4201	20	
Kern Front	8	3			2169	8	
Kern Front	8	4			2101	176	
Kern Front	8	5			1756	165	
Kern Front	8	6			2101	157	
Kern River	1	1			3174	170	
Kern River	1	2			2527	175	
Kern River	1	3			2106	89	
Kern River	1	4			1684	7	
Kern River	1	5			1846	20	
Kern River	2	1			1749	138	
Kern River	2	2			2462	144	
Kern River	3	1			1846	136	
Kern River	3	2			2106	137	
Kern River	4	1	100	85	3401	70	
Kern River	4	2			4470	74	
Kern River	5	1			2235	104	China Fault Zone
Kern River	5	2			3920	100	China Fault Zone
Kern River	5	3			1814	97	China Fault Zone
Kern River	5	4	60	100	2494	91	China Fault Zone
Kern River	5	5	100	135	2786	94	China Fault Zone

field	fault		apparent vertical offset		length (ft)	strike	note
	number	segment	start	end			
Kern River	5	6	135	160	2073	95	China Fault Zone
Kern River	5	7	60	40	2235	99	China Fault Zone
Kern River	5	8			2235	103	China Fault Zone
McClung	1	1			2335	69	
McClung	2	1	40	15	719	140	
McClung	2	2	15	60	609	140	
McClung	2	3	60	70	770	140	
McClung	2	4	70	5	1117	141	
McClung	2	5	15	20	1312	140	
McClung	2	6	20	20	1532	141	
McClung	2	7	20	20	1591	140	
McClung	3	1	80	45	1100	141	
McClung	3	2	45	65	1650	140	
McClung	3	3	80	80	85	140	
McClung	3	4	45	25	618	141	
McClung	3	5	25	15	643	140	
McClung	3	6	15	15	1159	140	
McClung	3	7	15	15	1134	139	
McClung	3	8	15	30	1345	140	
McClung	4	1	10	45	626	59	
McClung	5	1	15	10	762	47	
McClung	5	2	10	15	542	45	
McClung	5	3	15	20	1168	43	
McClung	5	4			440	40	
Mount Poso	1	1	130	130	2459	144	
Mount Poso	1	2	130	130	2317	147	
Mount Poso	1	3	80	75	2128	149	
Mount Poso	1	4	75	65	2932	150	
Mount Poso	2	1	20	20	2317	97	
Mount Poso	2	2	20	10	1560	106	
Mount Poso	2	3	10	5	1702	115	
Mount Poso	2	4	5	25	1749	124	
Mount Poso	2	5	25	30	1277	127	
Mount Poso	2	6	30	40	1324	132	
Mount Poso	3	1	80	80	2033	141	
Mount Poso	3	2	80	75	1277	144	
Mount Poso	3	3	65	75	2459	145	
Mount Poso	3	4	125	100	1608	145	
Mount Poso	3	5	125	140	4303	146	
Mount Poso	3	6	220	205	2080	162	
Mount Poso	3	7	240	240	567	167	
Mount Poso	3	8	250	250	662	168	
Mount Poso	3	9	265	230	993	4	
Mount Poso	3	10	230	170	2411	166	
Mount Poso	3	11	170	140	1135	152	
Mount Poso	3	12	220	240	2695	118	
Mount Poso	3	13	410	410	993	164	
Mount Poso	3	14	410	405	993	175	

field	fault		apparent vertical offset		length (ft)	strike	note
	number	segment	start	end			
Mount Poso	3	15	405	400	3121	156	
Mount Poso	3	16	400	405	1749	143	
Mount Poso	3	17	405	405	1371	156	
Mount Poso	3	18	405	410	1135	168	
Mount Poso	3	19	410	415	1513	175	
Mount Poso	3	20	415	415	615	160	
Mount Poso	3	21	120	110	1040	135	
Mount Poso	3	22	110	105	662	131	
Mount Poso	3	23	85	75	3073	147	
Mount Poso	3	24	75	80	1939	148	
Mount Poso	3	25	80	95	5012	141	
Mount Poso	3	26	95	95	1749	139	
Mount Poso	3	27	50	65	2080	136	
Mount Poso	3	28	65	70	804	126	
Mount Poso	4	1	55	55	2553	126	
Mount Poso	4	2	55	45	1844	127	
Mount Poso	4	3	15	75	2742	127	
Mount Poso	4	4	75	65	1324	130	
Mount Poso	4	5	55	35	1608	133	
Mount Poso	4	6	35	20	1844	153	
Mount Poso	4	7	20	10	1040	134	
Mount Poso	4	8	10	10	1939	133	
Mount Poso	4	9	20	5	1277	129	
Mount Poso	4	10	5	0	2175	130	
Mount Poso	5	1	60	60	4208	179	
Mount Poso	6	1	105	95	2695	136	
Mount Poso	6	2	120	105	3499	136	
Mount Poso	7	1	10	10	1324	175	
Mount Poso	7	2	195	215	2222	179	
Mount Poso	8	1	50	50	1844	117	
Mount Poso	8	2	50	40	1371	110	
Mount Poso	8	3	40	25	1040	111	
Mount Poso	8	4	25	5	1182	119	
Mount Poso	8	5	85	20	1088	129	
Mount Poso	8	6	20	20	1797	144	
Mount Poso	8	7	20	30	1371	104	
Mount Poso	9	1	90	40	3357	157	
Mount Poso	9	2	50	50	473	154	
Mount Poso	9	3	15	15	1135	160	
Mount Poso	9	4	30	30	473	158	
Mount Poso	10	1	45	70	4114	0	
Mount Poso	10	2	100	80	1749	0	
Mount Poso	11	1	70	100	2837	117	
Mount Poso	12	1	140	135	1939	114	
Mount Poso	12	2	50	65	1466	114	
Mount Poso	12	3	65	70	1702	116	
Mount Poso	12	4	70	80	1891	116	
Mount Poso	13	1	15	20	615	163	

field	fault		apparent vertical offset		length (ft)	strike	note
	number	segment	start	end			
Mount Poso	13	2	90	115	1844	157	
Mount Poso	13	3	115	125	662	147	
Mount Poso	13	4	125	150	993	130	
Mount Poso	13	5	150	160	615	136	
Mount Poso	13	6	160	170	804	153	
Mount Poso	14	1	70	90	1277	108	
Mount Poso	14	2	90	95	1608	122	
Mount Poso	14	3	95	95	1088	131	
Mount Poso	14	4	95	90	1560	145	
Mount Poso	14	5	90	100	1324	155	
Mount Poso	14	6	100	110	1466	162	
Mount Poso	14	7	110	140	3877	168	
Mount Poso	14	8	140	155	1797	163	
Mount Poso	14	9	155	165	1277	157	
Mount Poso	14	10	165	150	3263	155	
Mount Poso	14	11	150	145	851	152	
Mount Poso	14	12	145	130	1891	141	
Mount Poso	14	13	130	170	2932	135	
Mount Poso	14	14	170	165	2884	140	
Mount Poso	14	15	165	165	1182	146	
Mount Poso	14	16	165	140	2175	148	
Mount Poso	14	17	140	105	3594	155	
Mount Poso	14	18	35	30	898	156	
Mount Poso	14	19	40	45	2459	158	
Mount Poso	14	20	45	55	3546	162	
Mount Poso	15	1	130	100	1277	113	
Mount Poso	15	2	100	85	1891	120	
Mount Poso	15	3	85	95	2128	126	
Mount Poso	16	1	50	55	2742	157	
Mount Poso	16	2	40	20	993	147	
Mount Poso	16	3	175	150	2270	144	
Mount Poso	16	4	125	85	4114	145	
Mount Poso	16	5	85	75	3263	146	
Mount Poso	16	6	75	65	2175	148	
Mount Poso	16	7	65	110	4870	152	
Mount Poso	16	8	110	130	5059	151	
Mount Poso	16	9	130	150	4587	152	
Mount Poso	16	10	150	175	4681	152	
Mount Poso	16	11			1702	153	
Mount Poso	16	12			2506	158	
Mount Poso	17	1	155	130	1939	117	
Mount Poso	17	2	130	70	1608	133	
Mount Poso	17	3	70	50	3215	147	
Mount Poso	17	4	50	65	2080	136	
Mount Poso	17	5	65	120	2175	131	
Mount Poso	17	6	120	130	946	131	
Mount Poso	18	1	0	10	2884	145	
Mount Poso	18	2	10	0	2932	145	

field	fault		apparent vertical offset		length (ft)	strike	note
	number	segment	start	end			
Mount Poso	18	3	0	15	804	150	
Mount Poso	18	4	15	45	1891	154	
Mount Poso	18	5	45	65	1088	146	
Mount Poso	18	6	65	90	946	138	
Mount Poso	18	7	90	120	1324	135	
Mount Poso	18	8	120	130	1419	142	
Mount Poso	18	9	0	0	1419	148	
Mount Poso	19	1	55	50	615	0	
Mount Poso	19	2	50	40	1277	0	
Mount Poso	20	1	0	35	4303	148	
Mount Poso	20	2	35	40	2222	152	
Mount Poso	20	3	40	40	1419	140	
Mount Poso	20	4	40	55	1371	133	
Mount Poso	20	5	55	65	2033	124	
Mount Poso	20	6	65	60	2222	129	
Mount Poso	20	7	30	30	1513	142	
Mount Poso	20	8	30	50	1891	152	
Mount Poso	20	9	255	240	2411	157	
Mount Poso	20	10	240	170	6478	164	
Mount Poso	20	11	115	115	4634	163	
Mount Poso	21	1	35	35	378	98	
Mount Poso	21	2	95	100	2601	99	
Mount Poso	21	3	75	80	615	102	
Mount Poso	21	4	130	90	2506	110	
Mount Poso	21	5	90	80	1513	119	
Mount Poso	21	6	120	65	1229	129	
Mount Poso	21	7	65	105	3026	131	
Mount Poso	21	8	105	105	3121	138	
Mount Poso	21	9	105	95	3688	145	
Mount Poso	21	10	95	90	3641	144	
Mount Poso	21a	1	0	15	1229	123	
Mount Poso	21a	2	15	50	2411	128	
Mount Poso	21a	3	50	45	2459	134	
Mount Poso	21a	4	45	30	2080	139	
Mount Poso	22	1	10	10	1182	104	
Mount Poso	22	2	10	10	1324	110	
Mount Poso	22	3	45	25	1466	120	
Mount Poso	22	4	25	15	1655	120	
Mount Poso	22	5	15	15	1891	129	
Mount Poso	22	6	15	30	1797	135	
Mount Poso	22	7	230	220	2222	140	
Mount Poso	22	8	220	190	662	145	
Mount Poso	22	9	190	185	3641	142	
Mount Poso	22	10	185	190	3404	141	
Mount Poso	22	11	345	350	3073	140	
Mount Poso	22	12	350	350	3925	138	
Mount Poso	23	1	70	70	898	172	
Mount Poso	23	2	70	70	662	163	

field	fault		apparent vertical offset		length (ft)	strike	note
	number	segment	start	end			
Mount Poso	23	3	200	200	47	151	
Mount Poso	23	4	300	300	1419	148	
Mount Poso	23	5	300	300	1513	142	
Mount Poso	23	6	300	295	2411	139	
Mount Poso	23	7	405	430	4066	139	
Mount Poso	23	8	430	430	3073	139	
Mount Poso	24	1	105	110	1608	165	
Mount Poso	24	2	110	120	5390	168	
Mount Poso	24	3	120	120	1513	155	
Mount Poso	24	4	120	125	1844	147	
Mount Poso	24	5	125	110	1749	143	
Mount Poso	24	6	110	105	1229	152	
Mount Poso	24	7	105	90	1797	159	
Mount Poso	24	8	90	70	1371	160	
Mount Poso	24	9	70	50	1182	149	
Mount Poso	24	10	50	35	946	141	
Mount Poso	24	11	35	25	757	128	
Mount Poso	24	12	80	55	1229	116	
Mount Poso	24	13	55	25	1277	110	
Mount Poso	24	14	25	30	1844	115	
Mount Poso	24	15	30	30	1513	130	
Mount Poso	24	16	30	35	1371	139	
Mount Poso	24	17	35	35	1749	154	
Mount Poso	24	18	5	5	1466	163	
Mount Poso	24	19	5	0	1608	170	
Mount Poso	24	20	0	0	2648	1	
Mount Poso	25	1	0	45	1277	133	
Mount Poso	25	2	45	45	898	133	
Mount Poso	25	3	45	25	567	133	
Mount Poso	25	4	25	0	1560	133	
Mount Poso	26	1	25	25	520	172	
Mount Poso	26	2	25	20	1182	163	
Mount Poso	26	3	20	15	1088	156	
Mount Poso	26	4	15	20	1229	151	
Mount Poso	26	5	20	20	1277	148	
Mount Poso	26	6	20	0	2601	145	
Mount Poso	27	1	235	255	1513	128	
Mount Poso	27	2	255	240	993	131	
Mount Poso	28	1	155	140	3215	164	
Mount Poso	28	2	140	130	2884	167	
Mount Poso	29	1	295	285	2979	1	
Mount Poso	29	2	285	230	2553	0	
Mount Poso	29	3	290	170	2742	179	
Mount Poso	29	4	255	235	2411	177	
Mount Poso	29	5	245	230	3546	173	
Mount Poso	29	6	230	175	2175	168	
Mount Poso	30	1	45	45	378	120	
Mount Poso	30	2	45	30	1040	126	

field	fault		apparent vertical offset		length (ft)	strike	note
	number	segment	start	end			
Mount Poso	30	3	30	20	993	131	
Mount Poso	30	4	20	20	804	139	
Mount Poso	30	5	20	15	1040	148	
Mount Poso	30	6	70	90	993	160	
Mount Poso	31	1	55	55	615	141	
Mount Poso	31	2	55	60	2033	145	
Mount Poso	31	3	60	60	1702	151	
Mount Poso	31	4	60	75	1182	158	
Mount Poso	31	5	75	85	1040	168	
Mount Poso	32	1	55	85	1371	1	
Mount Poso	32	2	85	90	567	165	
Mount Poso	32	3	90	125	2411	158	
Mount Poso	32	4	125	140	1371	163	
Mount Poso	32	5	95	110	1560	166	
Mount Poso	32	6	110	125	1702	173	
Mount Poso	33	1	110	105	2175	14	
Mount Poso	33	2	105	105	1608	15	
Mount Poso	33a	1	115	115	3452	157	
Mount Poso	33a	2	115	110	2506	154	
Mount Poso	34	1	45	30	1749	177	
Mount Poso	34	2	30	15	1749	174	
Mount Poso	34	3	15	5	1419	172	
Mount Poso	34	4	105	75	1655	170	
Mount Poso	35	1	50	50	189	59	
Mount Poso	35	2	90	90	1419	59	
Mount Poso	35	3	90	85	1324	58	
Mount Poso	35	4	85	75	1054	58	
Mount Poso	35	5	65	60	236	58	
Mount Poso	35	6	20	25	426	58	
Mount Poso	36	1	30	0	1466	79	
Mount Poso	36	2	105	185	1891	79	
Mount Poso	37	1	0	20	851	60	
Mount Poso	37	2	20	25	1371	57	
Mount Poso	37	3	25	15	1324	60	
Mount Poso	37	4	15	15	1513	61	
Mount Poso	38	1	75	70	1797	43	
Mount Poso	38	2	70	50	804	42	
Mount Poso	38	3	50	50	2080	43	
Mount Poso	39	1			1040	119	
Mount Poso	40	1			757	117	
Mount Poso	41	1	0	0	2317	5	
Mount Poso	42	1	80	85	757	95	
Mount Poso	42	2	85	90	2080	99	
Mount Poso	43	1	65	65	2317	61	
Mount Poso	44	1	0	5	520	97	
Mount Poso	44	2	5	5	2317	97	
Mount Poso	45	1	90	90	851	90	
Mount Poso	45	2	90	85	1277	90	

field	fault		apparent vertical offset		length (ft)	strike	note
	number	segment	start	end			
Mount Poso	45	3	85	100	1939	91	
Mount Poso	45	4	50	50	1135	90	
Mount Poso	45	5	50	65	1324	86	
Mount Poso	45	6	65	20	851	77	
Mount Poso	45	7	85	110	1135	68	
Mount Poso	46	1	15	40	1608	76	
Mount Poso	46	2	40	35	473	74	
Mount Poso	46	3	25	30	3499	75	
Mount Poso	46	4	25	25	236	75	
Mount Poso	46	5	15	15	662	75	
Mount Poso	46	6	25	25	3404	75	
Mount Poso	47	1	105	105	1466	82	
Mount Poso	47	2	175	195	1844	80	
Mount Poso	47	3	55	15	2790	79	
Mount Poso	47	4	15	5	1844	78	
Mount Poso	47	5	20	30	804	76	
Mount Poso	48	1	100	120	1371	55	
Mount Poso	48	2	65	60	1466	58	
Mount Poso	48	3	60	15	1608	57	
Mount Poso	49	1	0	20	1182	54	
Mount Poso	49	2	20	0	709	54	
Mount Poso	50	1	260	270	2317	23	
Mount Poso	51	1	100	100	6147	98	
Mount Poso	52	1	110	115	1797	50	
Mount Poso	52	2	115	115	2601	51	
Mount Poso	53	1	0	25	520	60	
Mount Poso	53	2	210	205	1182	64	
Mount Poso	54	1	110	120	1088	60	
Mount Poso	54	2	120	100	2364	60	
Mount Poso	55	1	85	120	2459	35	
Mount Poso	55	2	120	110	2790	34	
Mount Poso	56	1	55	55	1466	64	
Mount Poso	57	1	70	75	2742	81	
Mount Poso	57	2			1797	84	
Mount Poso	58	1	45	45	1655	37	
Mount Poso	58	2	45	45	1844	44	
Mount Poso	58	3	45	45	1797	48	
Mount Poso	59	1	660	660	2648	71	
Mount Poso	59	2	570	585	2459	75	
Mount Poso	59	3	630	625	1655	78	
Mount Poso	59	4	625	620	1560	79	
Mount Poso	59	5	620	615	1135	84	
Mount Poso	59	6	730	745	1513	84	
Mount Poso	59	7	745	765	1891	88	
Mount Poso	59	8	465	780	2128	89	
Mount Poso	59	9	640	615	473	87	
Mount Poso	59	10	455	470	1182	86	
Mount Poso	59	11	295	300	1419	83	

field	fault		apparent vertical offset		length (ft)	strike	note
	number	segment	start	end			
Mount Poso	59	12	410	410	804	81	
Mount Poso	59	13	300	295	804	84	
Mount Poso	59	14	295	290	757	92	
Mount Poso	59	15	290	295	1371	99	
Mount Poso	59	16	400	385	1371	106	
Mount Poso	59	17	385	365	1844	114	
Mount Poso	59	18	290	295	1939	120	
Mount Poso	59	19	295	300	2222	121	
Mount Poso	60	1	40	65	1182	153	
Mount Poso	60	2	175	160	2175	162	
Mount Poso	61	1	105	105	1229	85	
Mount Poso	61	2	105	100	1466	75	
Mount Poso	62	1	265	270	1324	51	
Mount Poso	62	2	270	275	1277	55	
Mount Poso	62	3	275	280	1229	62	
Mount Poso	62	4	280	300	1324	71	
Mount Poso	63	1	235	230	1135	44	
Mount Poso	63	2	230	220	1324	44	
Mount Poso	63	3	180	180	1513	53	
Mount Poso	64	1	90	90	851	21	
Mount Poso	64	2	95	95	851	30	
Mount Poso	64	3	100	100	757	34	
Mount Poso	64	4	105	105	757	41	
Mount Poso	64	5	110	110	946	54	
Poso Creek	1	1			1068	118	
Poso Creek	1	2			1437	123	
Poso Creek	1	3			2358	129	
Poso Creek	1	4			847	125	
Poso Creek	1	5	245	295	2431	120	
Poso Creek	1	6	295	330	2247	123	
Poso Creek	1	7	140	160	1289	127	
Poso Creek	1	8	160	225	1768	127	
Poso Creek	1	9	265	315	1031	129	
Poso Creek	1	10			3684	126	
Poso Creek	2	1			1584	122	
Poso Creek	3	1			553	128	
Poso Creek	3	2			1510	133	
Poso Creek	3	3			921	122	
Poso Creek	4	1	15	0	1437	168	
Poso Creek	4	2	0	5	442	167	
Poso Creek	4	3	5	25	1289	164	
Poso Creek	4	4			1068	167	
Poso Creek	4	5	20	15	5489	160	
Poso Creek	4	6	15	15	626	169	
Poso Creek	4	7	15	10	553	173	
Poso Creek	4	8	10	5	663	178	
Poso Creek	4	9	5	0	921	5	
Poso Creek	5	1	10	20	1105	157	

field	fault		apparent vertical offset		length (ft)	strike	note
	number	segment	start	end			
Poso Creek	5	2	20	0	1695	155	
Poso Creek	5	3	20	50	1879	152	
Poso Creek	5	4	50	60	1510	147	
Poso Creek	5	5	60	70	1510	140	
Poso Creek	6	1	260	230	1695	177	
Poso Creek	6	2	230	190	2173	1	
Poso Creek	6	3	190	165	1584	5	
Poso Creek	6	4	165	120	1805	4	
Poso Creek	6	5	120	85	1252	178	
Poso Creek	6	6	85	25	1695	174	
Poso Creek	6	7	25	65	921	169	
Poso Creek	6	8	65	50	1363	166	
Poso Creek	6	9	50	35	1031	157	
Poso Creek	6	10	35	20	1326	149	
Poso Creek	6	11	20	15	553	160	
Poso Creek	6	12	15	20	295	169	
Poso Creek	6	13	20	30	1252	7	
Poso Creek	6	14	30	0	1068	6	
Poso Creek	6	15	0	15	1437	3	
Poso Creek	6	16	15	50	810	0	
Poso Creek	6	17	50	85	995	175	
Poso Creek	6	18	85	90	810	169	
Poso Creek	6	19	90	105	1547	163	
Poso Creek	6	20	105	120	1658	155	
Poso Creek	7	1	40	30	1473	175	
Poso Creek	7	2	30	15	1216	178	
Poso Creek	7	3	15	5	516	0	
Poso Creek	7	4	5	95	2284	0	
Poso Creek	7	5	95	130	4568	179	
Poso Creek	7	6	130	120	2836	175	
Poso Creek	7	7	120	115	2100	178	
Poso Creek	7	8	115	65	2284	0	
Poso Creek	7	9	65	70	958	0	
Poso Creek	7	10	70	40	1879	2	
Poso Creek	7	11	40	30	1289	2	
Poso Creek	7	12	30	20	1142	0	
Poso Creek	7	13	140	140	2726	0	
Poso Creek	7	14	140	140	2947	178	
Poso Creek	7	15			884	178	
Poso Creek	8	1			2394	175	
Poso Creek	8	2			2652	177	
Poso Creek	8	3			2100	178	
Poso Creek	8	4	20	15	1805	179	
Poso Creek	8	5	15	0	2984	1	
Poso Creek	9	1			1473	160	
Poso Creek	9	2			2468	165	
Poso Creek	9	3			1216	166	
Poso Creek	9	4			1252	169	

field	fault		apparent vertical offset		length (ft)	strike	note
	number	segment	start	end			
Poso Creek	9	5			1547	172	
Poso Creek	9	6			1621	175	
Poso Creek	10	1	0	10	553	85	
Poso Creek	10	2	10	10	995	85	
Poso Creek	11	1	0	10	332	112	
Poso Creek	11	2	10	10	368	112	
Poso Creek	11	3	10	0	553	112	
Poso Creek:McVan	1	1			631	118	
Poso Creek:McVan	1	2			501	125	
Poso Creek:McVan	1	3			305	132	
Poso Creek:McVan	2	1			2885	146	
Poso Creek:McVan	3	1			4268	33	
Poso Creek:McVan	4	1			446	123	
Poso Creek:McVan	5	1			4072	31	
Poso Creek:McVan	6	1			631	122	
Poso Creek:McVan	6	2			664	131	
Poso Creek:McVan	6	3			1165	141	
Poso Creek:McVan	6	4			457	147	
Poso Creek:McVan	6	5			697	154	
Poso Creek:McVan	6	6			871	161	
Poso Creek:McVan	6	7			849	163	
Poso Creek:McVan	6	8			1100	166	
Poso Creek:McVan	6	9			1285	168	
Poso Creek:McVan	7	1	70	65	980	148	
Poso Creek:McVan	7	2	65	60	588	153	
Poso Creek:McVan	7	3	60	55	490	162	
Poso Creek:McVan	7	4	55	50	1176	174	
Poso Creek:McVan	7	5	50	100	762	175	
Poso Creek:McVan	7	6	100	85	1132	177	
Poso Creek:McVan	7	7			980	178	
Poso Creek:McVan	8	1			523	130	
Poso Creek:McVan	8	2			631	139	
Poso Creek:McVan	8	3			403	145	
Poso Creek:McVan	8	4			1012	148	
Poso Creek:McVan	8	5			708	155	
Poso Creek:McVan	9	1			599	165	
Poso Creek:McVan	9	2			1644	169	
Rio Bravo	1	1			386	6	
Rio Bravo	1	2	10	5	134	6	
Rio Bravo	1	3	5	0	252	6	
Rio Bravo	1	4	0	0	185	6	
Rio Bravo	1	5	0	5	168	6	
Rio Bravo	1	6	5	0	117	6	
Rio Bravo	1	7	0	5	117	6	
Rio Bravo	1	8	5	25	654	6	
Rio Bravo	1	9	25	10	302	4	
Rio Bravo	1	10	10	5	839	4	
Rio Bravo	1	11	5	5	1426	3	

field	fault		apparent vertical offset		length (ft)	strike	note
	number	segment	start	end			
Rio Bravo	1	12	5	0	755	2	
Rio Bravo	2	1			587	3	
Rio Bravo	2	2	70	115	252	3	
Rio Bravo	2	3	115	135	235	3	
Rio Bravo	2	4	135	135	218	3	
Rio Bravo	2	5	135	145	235	3	
Rio Bravo	2	6	145	135	268	3	
Rio Bravo	2	7	135	150	336	3	
Rio Bravo	2	8	150	150	319	3	
Rio Bravo	2	9	150	140	436	3	
Rio Bravo	2	10	140	90	520	3	
Rio Bravo	2	11	90	70	872	3	
Rio Bravo	2	12	70	40	621	0	
Rio Bravo	2	13	40	25	302	0	
Rio Bravo	2	14	25	20	721	0	
Rio Bravo	2	15	20	15	755	0	
Rio Bravo	2	16	15	0	788	0	
Rio Bravo	3	1			1527	146	
Rio Bravo	3	2			1241	148	
Rio Bravo	3	3			1409	151	
Rio Bravo	3	4			1963	152	
Rosedale	1	1			1201	2	
Rosedale	1	2	90	60	1327	3	
Rosedale	1	3	60	40	1255	2	
Rosedale	1	4	40	50	1381	3	
Rosedale	1	5			1829	2	
Rosedale	2	1			2349	166	Rosedale Fault
Rosedale	2	2			717	169	Rosedale Fault
Rosedale	2	3			251	172	Rosedale Fault
Rosedale	2	4	70	100	1685	178	Rosedale Fault
Rosedale	2	5	100	60	1112	178	Rosedale Fault
Rosedale	2	6	60	100	1506	179	Rosedale Fault
Rosedale	2	7	100	85	484	2	Rosedale Fault
Rosedale	2	8	85	70	520	9	Rosedale Fault
Rosedale	2	9	215	140	520	7	Rosedale Fault
Rosedale	2	10	140	90	377	2	Rosedale Fault
Rosedale	2	11	90	30	412	175	Rosedale Fault
Rosedale	2	12			914	176	Rosedale Fault
Rosedale	2	13			753	179	Rosedale Fault
Rosedale	3	1			484	2	Bellevue Fault
Rosedale	3	2			663	7	Bellevue Fault
Rosedale	3	3			2994	13	Bellevue Fault
Rosedale	3	4			502	21	Bellevue Fault
Rosedale	3	5			556	30	Bellevue Fault
Rosedale	3	6			269	28	Bellevue Fault
Rosedale	3	7			520	23	Bellevue Fault
Rosedale	3	8			1667	2	Bellevue Fault
Rosedale	3	9			466	178	Bellevue Fault

field	fault		apparent vertical offset		length (ft)	strike	note
	number	segment	start	end			
Rosedale	3	10			645	171	Bellevue Fault
Rosedale	3	11			645	165	Bellevue Fault
Rosedale	3	12			4321	170	Bellevue Fault
Rosedale	4	1	40	35	233	47	
Rosedale	4	2	35	25	610	47	
Rosedale	4	3	25	10	1649	47	
Rosedale	4	4	10	0	412	47	
Rosedale	5	1	140	95	2080	141	
Rosedale Ranch	1	1	30	35	396	158	
Rosedale Ranch	1	2	35	45	960	160	
Rosedale Ranch	1	3	45	55	1200	164	
Rosedale Ranch	1	4	55	50	2424	167	
Rosedale Ranch	2	1	30	30	768	1	
Rosedale Ranch	2	2	30	30	1044	5	
Rosedale Ranch	2	3	30	30	1116	9	
Rosedale Ranch	2	4	30	30	336	9	
Rosedale Ranch	2	5	25	25	636	14	
Rosedale Ranch	2	6	25	25	444	18	
Rosedale Ranch	2	7	25	5	2256	19	
Rosedale Ranch	2	8	5	0	828	20	
Rosedale Ranch	3	1			2988	164	
Rosedale Ranch	3	2			540	165	
Rosedale Ranch	3	3			444	170	
Rosedale Ranch	3	4			444	174	
Rosedale Ranch	3	5			1032	1	
Rosedale Ranch	3	6			960	4	
Rosedale Ranch	3	7			1260	5	
Rosedale Ranch	4	1			864	163	
Rosedale Ranch	4	2			720	159	
Rosedale Ranch	4	3			636	157	
Rosedale Ranch	4	4			528	159	
Rosedale Ranch	4	5			624	165	
Rosedale Ranch	4	6			720	176	
Rosedale Ranch	4	7			660	174	
Rosedale Ranch	4	8			720	177	
Rosedale Ranch	4	9			768	0	
Rosedale Ranch	4	10			744	2	
Rosedale Ranch	4	11			1092	4	
Rosedale Ranch	5	1	40	25	2280	167	
Rosedale Ranch	5	2	25	15	648	166	
Rosedale Ranch	5	3	15	5	420	169	
Rosedale Ranch	5	4	5	10	696	176	
Rosedale Ranch	5	5	10	10	708	1	
Rosedale Ranch	5	6	10	10	720	5	
Rosedale Ranch	5	7	10	10	984	7	
Rosedale Ranch	5	8	10	10	732	9	
Rosedale Ranch	5	9	10	10	924	14	
Rosedale Ranch	6	1			684	179	

field	fault		apparent vertical offset		length (ft)	strike	note
	number	segment	start	end			
Rosedale Ranch	6	2			852	2	
Rosedale Ranch	6	3			708	1	
Rosedale Ranch	6	4			588	179	
Rosedale Ranch	6	5			684	177	
Rosedale Ranch	6	6			708	171	
Rosedale Ranch	6	7			720	167	
Rosedale Ranch	6	8			612	163	
Rosedale Ranch	6	9			660	158	
Rosedale Ranch	7	1	0	20	1008	39	
Rosedale Ranch	7	2	30	10	720	41	
Rosedale Ranch	7	3	10	0	204	41	
Rosedale Ranch	7	4	0	5	216	41	
Seventh Standard	1	1	330	330	614	169	
Seventh Standard	1	2	330	330	444	175	
Seventh Standard	1	3	330	335	2476	0	
Seventh Standard	1	4	335	335	936	2	
Seventh Standard	1	5	335	335	1909	0	
Shafter	1	1	20	20	1178	143	
Shafter	1	2	20	0	1217	146	
Shafter	1	3	0	30	2552	147	
Shafter	1	4	30	60	2100	152	
Shafter	1	5	60	90	2100	156	
Shafter	1	6	90	90	2983	160	
Shafter	1	7	90	90	2316	163	
Shafter	1	8	90	90	2611	165	
Shafter Southeast Gas	1	1			6046	148	
Shafter Southeast Gas	1	2	11	3	3015	148	
Shafter Southeast Gas	1	3	20	20	3553	147	
Shafter Southeast Gas	1	4			2119	147	
Shafter Southeast Gas	2	1	20	20	5476	17	
Shafter Southeast Gas	2	2	20	17	2004	16	
Strand	1	1			3710	55	
Strand	1	2			3869	54	
Strand	1	3			4825	52	
Strand	1	4			1775	51	
Strand	2	1	0	10	1206	62	
Strand	2	2	10	10	1525	62	
Strand	2	3	10	0	956	60	
Strand	2	4	0	5	341	59	
Strand	2	5	5	0	137	59	
Strand	2	6	0	20	569	59	
Strand	2	7	20	25	1320	59	
Strand	2	8	25	25	523	59	
Strand	3	1	90	60	2390	169	
Strand	3	2	15	20	2390	169	
Strand	3	3	20	0	660	169	
Strand	3	4	0	5	273	169	
Strand	3	5	40	60	432	165	

field	fault		apparent vertical offset		length (ft)	strike	note
	number	segment	start	end			
Strand	3	6	60	35	387	165	
Strand	3	7	35	20	387	165	
Strand	3	8	20	0	660	165	
Strand	3	9	0	5	614	165	
Strand	3	10	5	10	1593	165	
Strand	3	11	10	15	910	165	
Strand	3	12	15	20	2208	165	
Strand	3	13	20	20	1616	165	
Strand	4	1	50	70	728	58	
Strand	4	2	70	50	637	58	
Strand	4	3	50	10	1024	58	
Strand	5	1			6236	152	
Strand	5	2	5	30	1206	152	
Strand	5	3	30	10	3209	152	
Strand	5	4	10	15	1730	153	
Strand	5	5	15	5	2185	153	
Strand	6	1	45	20	933	69	
Strand	6	2	20	15	592	69	
Strand	6	3	15	25	387	69	
Strand	6	4	25	40	1138	69	
Strand	7	1			1001	73	
Strand	7	2			1388	68	
Strand	7	3			1457	63	
Strand	7	4			910	59	
Strand	7	5	10	0	205	59	
Strand	7	6	0	10	205	59	
Strand	7	7	10	5	546	57	
Strand	7	8	5	5	614	55	
Strand	7	9			1001	54	
Strand	7	10			933	50	
Strand	8	1	10	15	523	125	
Strand	8	2	15	55	660	125	
Strand	8	3	55	100	546	125	
Strand	8	4	100	125	592	125	
Strand	8	5	125	145	523	125	
Strand	9	1	0	0	1161	78	
Strand	9	2	0		774	84	
Strand	9	3			1297	76	
Strand	9	4			1525	71	
Strand	9	5		10	1752	65	
Strand	9	6	10	10	1183	63	
Strand	9	7	10	10	432	60	
Strand	9	8	10	35	910	59	
Strand	9	9	35	105	1115	59	